

UNIVERSITA' DEGLI STUDI DI NAPOLI FEDERICO II



FACOLTA' DI INGEGNERIA

PhD in Materials and Structures Engineering

- XXVI Cycle -20014

ENGINEERING TUNABLE TEMPERATURE AND
pH RESPONSIVE PNIPAM-VAA MICROGELS FOR
BIOMEDICAL APPLICATIONS

Antonio Papa

Advisor

Prof. Paolo Antonio Netti

Department of Materials Engineering and Production

Abstract

Sensing and recognition of bio-molecules is of extreme interest nowadays because it allows for detection of specific targets which can be the hallmarks of diseases. Colloidal particles can be used as a powerful platform to recognize bio-molecules and to perform a fast screening of them. Indeed, in most cases the surface of colloidal particles can be easily functionalized with agents which allow to control specific interaction between the particles and specific recognition. In addition, colloids with a switchable recognition mechanism, which can be externally triggered, would have a tremendous impact in the field of drug delivery and bio-sensing.

“Smart” microgels are potentially suitable for these applications. They are extensively studied due to their swelling response to changes in specific environmental stimuli (*i.e.* pH, temperature, solute concentration, solvent composition, ionic strength, light, or electric field). While a variety of polymer systems have been explored, most attention has focused on microgels based on *poly(N-isopropylacrylamide)* (PNIPAM). They exhibit an extreme response to changes in temperature. Linear PNIPAM has a lower critical solution temperature (LCST) of 32 °C in aqueous solution, at which point the polymer reversibly switches from a fully soluble, hydrophilic random coil at lower temperatures to an insoluble globule at higher temperatures. When cross-linked into a colloidal gel, PNIPAM-based microgels exhibit this temperature responsiveness by undergoing a reversible de-swelling volume phase transition between 32 and 35 °C (the volume phase transition temperature, VPTT).

Smart environmental triggers can be incorporated into the PNIPAM microgels by co-polymerization, to provide multivariable control over the

particle swelling like temperature and pH. The functionalization of PNIPAM microgels with carboxylic acid groups can provide these properties and can achieve several objectives. The VPTT behavior of the microgel can be controlled *via* carboxylic groups incorporation. Both the value of the VPTT and the breadth of the deswelling transition can be influenced through copolymerization of more hydrophilic monomers. Functionalization can also provide reactive sites for post-modification of the gel, such as the bioconjugation of ligands.

Our work has consisted in synthesizing tunable thermo- and pH-responsive core-shell microgels based on *N*-Isopropylacrylamide (NIPAM) coupled with vinyl acetic acid (VAA) groups. Their volume sensitivity to pH and temperature were monitored by small-angle neutron scattering (SANS) and light scattering measurements. Ultra-structural analysis revealed core-shell architecture of the microgels with the core consisting of PNIPAM while the shell composed by PNIPAM and VAA. Volume change of the microgel in response to environmental pH and temperature were driven by separate mechanisms. Temperature sensitivity is conveyed mainly by the PNIPAM component while the pH sensitivity was imparted by the VAA component. As consequence, pH volume changes affected mainly the outer shell whereas the temperature volume change is localized both in the core and in the shell. Results indicated that by changing relative composition of NIPAM and VAA it is possible to tune the microgel VPTT and by changing the relative extension of core and shell compartment it is possible to tune the sensitivity of the gel to the environmental variation.

Afterwards, we set out to investigate whether DNA conjugated microgels were compatible with hybridization process, which is commonly used for manipulations of DNA in the design of DNA bioassays or biosensors. First, we performed a Quenching experiment, in order to investigate the nature of the interaction of DNA fragments with microgel (physisorption *vs* hybridization) and thus, the specificity of hybridization on microgels.

Cy5-labeled DNA oligonucleotide was conjugated with PNIPAM-VAA particles and by using a full complementary DNA oligonucleotide, opportunely modified with Black Hole Quencher 2 (BHQ-2), we performed the quenching experiment. Once confirmed the capability of DNA conjugated microgels to catch and recognize specifically complementary DNA strands we analyzed the effect of temperature and pH on the hybridization event and its stability.

The hybridization process was performed and tested in terms of specific catching of a complementary oligonucleotide and successively, it was studied in details, looking at the effect of microgel structural changes.

The effect of the shrinkage controlled by temperature changes does not drive any de-hybridization process. No dependence of the hybridization process was highlighted during microgel conformation changing, neither when the shell has collapsed nor when it is fully extended outside the microgel. Even analyzing the process as function of the oligonucleotide exposure towards the complementary oligo sequence, there is no direct evidence of its effects on the interaction process between the two DNA strands.

Eventually, DNA conjugated PNIPAM-VAA microgels charge properties were exploited for a reproducible and facile approach optimized for physisorption of gold nanoparticles. The advance of this approach consists in the simple mechanism by which gold nanoparticles are adsorbed on microgels templates, without dealing with sophisticated chemical treatment for their conjugation with the microgel. The resulted PNIPAAm-40nm gold nanoparticles modes demonstrate that this approach provides the capability to tune the interparticle distance and therefore to control and modulate the Surface Enhanced Raman Spectroscopy (SERS) affinity upon temperature changing.

Table of Contents

CONTENTS

Chapter I: Introduction

1.1 Temperature sensitive PNIPAM based microgels	1
1.2 Thermo- and pH-responsive PNIPAM microgels with carboxylic groups 4	
1.3 Swelling process of PNIPAM based microgels	6
1.4 Biomedical applications of PNIPAM microgels	8
1.4.1 PNIPAM microgels for drug delivery	8
1.4.2 PNIPAM microgels for biosensing	13
References	15

Chapter II: Engineering tunable temperature and pH responsive PNIPAM-VAA core-shell microgel particles

Introduction	20
2.1 Materials and methods.....	22
2.1.1 Materials	22
2.1.2 Microgel Preparation	22
2.1.3 TEM micrographs.....	23
2.1.4 Light Scattering experiments.....	23
2.1.5 Dynamic Light Scattering Analysis	24
2.1.6 Small Angle Neutron Scattering experiments	25
2.1.7 Small Angle Neutron Scattering and Static Light Scattering Analysis	25

2.2 Results and discussion.....	27
2.2.1 Transmission electron micrographs.....	27
2.2.2 Hydrodynamic radii and swelling ratio	28
2.2.3 Structure of VAA-particles	30
2.2.4 Small Angle Neutron Scattering.....	31
2.2.5 Static light scattering	33
Conclusions	36
References	37
Chapter III: DNA hybridization process on PNIPAM-VAA microgels particles	
Introduction	39
3.1 Materials and methods.....	41
3.1.1 Materials.....	41
3.1.2 DNA conjugation on PNIPAM-VAA microgel particles	42
3.1.3 Spectrofluorimetry.....	43
3.1.4 Quenching experiments on Cy5-DNA coupled PNIPAM-VAA microgels particles.....	44
3.1.5 Hybridization on PNIPAM-VAA microgel coupled with Cy5-DNA	45
3.1.6 CLSM imaging for fluorescence quantification.....	45
3.1.7 Dynamic Light Scattering Microgel Characterization	46
3. 2 Results and discussion: Study of the hybridization process on PNIPAM-VAA microgels.....	47
3.2.1 Hydrodynamic Radii	48

3.2.2 Cy5-DNA conjugated PNIPAM-VAA microgels capability in catching specific DNA oligonucleotides: hybridization or adsorption?.....	50
3.2.3 Effect of temperature on on Cy5-DNA conjugated PNIPAM-VAA microgels hybridization.....	51
Conclusions	54
References	55
Chapter IV: High efficient SERS substrate formulation by self-assembled gold nanoparticles physisorbed on PNIPAM thermoresponsive hydrogels	
Introduction	58
4.1 Materials and methods.....	60
4.1.1 Materials.....	60
4.1.2 DNA coupling reaction with PNIPAM-VAA microgels and absorption of gold nanoparticles	61
4.1.3 UV-Vis absorption spectroscopic measurements.....	61
4.1.4 Dynamic Light Scattering measurements	62
4.1.5 TEM micrographs.....	62
4.1.6 Raman spectroscopy.....	62
4.2 Results and Discussion.....	63
Conclusions	Error! Bookmark not defined.
References	73

CHAPTER I

Introduction

1.1 TEMPERATURE SENSITIVE PNIPAM BASED MICROGELS

Microgels are colloidally stable hydrogels whose size can vary from tens of nanometers to micrometers. Baker first coined the term “microgel” in literature, where the word “micro” referred to the size of the gel particles, while “gel” to the ability of a particle to swell in organic solvents [1]. Microgels behave much like hydrophobic colloids on a macroscopic level; they can be flocculated by the addition of salt or polymeric flocculant and they can be readily characterized by standard colloid techniques such as electrophoresis and dynamic light scattering. Structurally microgels resemble a three-dimensional, covalently cross-linked network and can swell in good solvents. On this microscopic level, microgels behave much like a conventional hydrogel and can be described in terms of their water content, average cross-link density, and characteristic time constants for swelling and deswelling. This superposition of the favorable properties of gels (i.e., elasticity, solvent retention, and dimensional stability) within the small dimensions of colloidal particles (facilitating faster swelling kinetics and the formation of ordered arrays) has made microgels of great interest in

industries such as cosmetics, coatings, lubricants, food oil recovery, drug delivery, biotechnology, and industrial processing.

In recent years, considerable interest has been focused on the development of “smart” aqueous microgels, whose properties change dramatically upon the application of specific environmental stimuli. While a variety of polymer systems have been explored [2], most attention has focused on microgels based on poly(N-isopropylacrylamide) (PNIPAM), argument of this work. PNIPAM-based properties display extreme temperature sensitivity in water. The basic structure of NIPAM is shown in Figure 1.1. PNIPAM microgels are cross-linked monodisperse colloidal dispersions and are readily synthesized by free-radical precipitation polymerization [3]. The particle size can be easily tuned with size distribution very narrow. They are composed by NIPAM, which is a polymer having a lower critical solution temperature (LCST) in water of $\sim 32^{\circ}\text{C}$ [3, 4, 5]. All the microgel properties are sensitive functions of temperature in the range of $15\text{-}50^{\circ}\text{C}$. The thermosensitivity of PNIPAM based aqueous microgels is inherited by gels made of PNIPAM. These microgels exhibit a volume phase transition temperature (VPTT) [6] at around the LCST of PNIPAM. The essential temperature-sensitive properties are illustrated in Figure 1.2. At room temperature, the microgel particle is swollen with water content, by a lower refractive index difference with water and a few electrically charged groups on the chain ends. At temperatures higher than the VPTT microgel particle shrinks, passing to a compact state (relatively hydrophobic); most of water content is released, the density of electrically charged groups is higher and the refractive index difference with water gets greater.

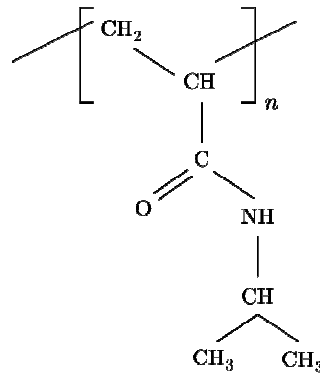


Figure 1.1: Formula of a PNIPAM molecule.

VPTT of PNIPAM microgel is close to the body temperature, and the responsive behavior of PNIPAM can be tuned to deswell at any given temperature simply by incorporation of monomers with differing hydrophobicity and hydrophilicity values [7]. As result, the ability to modulate changes in the microgels particle size (and thus also the water content and pore size) in addition to the thermo-responsivity, let PNIPAM based aqueous microgels hold considerable potential in applications that demand environmentally triggered changes or “switchable/intelligent” materials [8, 9, 10]. Because of these unique proprieties, PNIPAM microgel has found numerous applications in biomedical areas. The most important research fields in this ambit are drug delivery [11], biomolecules immobilization and absorption [12], and sensors [13].

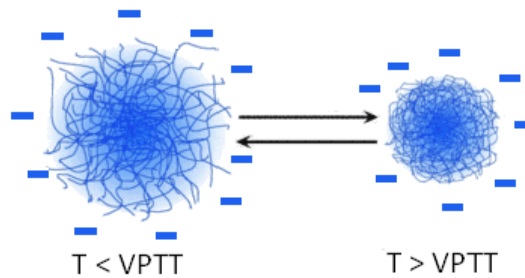


Figure 1.2: A schematic illustration of a PNIPAM microgel swelling.

1.2 THERMO- AND pH-RESPONSIVE PNIPAM MICROGELS WITH CARBOXYLIC GROUPS

Smart environmental triggers can be incorporated into the gel by copolymerization, to provide multivariable control over the particle swelling. The responsive behavior of PNIPAM can be extended to react on further stimuli as, *e.g.* ionic strength [14], solvent composition [15], radiation [16], selective reaction [17], and pH [18]. Carboxylic-acid-functionalized microgels based on PNIPAM exhibit reversible volumetric swelling response to the application of both thermal and pH stimuli. Carboxylic groups are pH ionizable, they produce electrophilic sites that, when ionized, increase the osmotic pressure inside the particle retarding the VPTT of the microgel. The versatility of the thermo- and pH-responsive microgels enhances the number of potential applications. In fact, the functionalization of PNIPAM microgels with carboxylic acid groups can achieve several objectives. The VPTT behavior of the microgel can be controlled via carboxylic groups incorporation. Both the value of the VPTT and its breadth of the deswelling transition can be influenced through copolymerization of more hydrophilic monomers. Functionalization can also provide reactive sites for post-modification of the gel, such as the bioconjugation of ligands.

The total number of carboxylic groups and their distribution within the microgel play an important role in controlling its swelling behavior. The distribution of carboxylic groups strongly affects both the local charge density and the average chain length of PNIPAM, both of which have been found to influence the onset VPTT and the breadth of the volume phase transition [2, 19]. In addition, the distribution and the accessibility of the carboxylic groups are critical in determining the types of applications suitable for a particular microgel. Microgel suited for bioconjugation would contain carboxylic groups at or near to the particle surface which are readily

accessible for subsequent chemical reactions, while microgels targeted for drug delivery applications would ideally contain internal functional groups whose access is diffusion-controlled.

The distribution of carboxylic groups had much attention in literature, since it is very important for predicting the volume phase transition behavior and the applicability of microgel systems. Zhou and Chu [19] performed studies over a broad range of methacrylic acid (MAA)/NIPAM copolymer microgel. For MAA/NIPAM ratios in the range of 10%, they proposed a core-shell microstructure model in which a MAA-enriched shell exists surrounding a NIPAM-enriched core. Kokufuta [20, 21] carried out similar investigations on an acrylic acid (AA)/NIPAM copolymer microgel with extremely high acrylic acid content (30%) and concluded that the bulk of charges did not reside on the particle surface.

However, both copolymerization kinetics [22] and experimental observations [18] indicate that AA and MAA tend to form blocks within the NIPAM-rich polymer chains. Carboxylated monomers blocks inside the NIPAM-rich chains increase the pK_a of the directly adjacent acid group, decreasing the sensitivity to pH stimuli. This particular behavior is known as polyelectrolyte effect [23]. In addition a high concentration of functional monomer decreases the NIPAM fraction and subsequently the temperature sensitivity.

On the basis of these considerations, Pelton introduced multiresponsive microgels with a kind of “core-shell” morphology preparing microgels based on PNIPAM functionalized with vinylacetic acid (VAA) [18]. Its morphology consists in a NIPAM-rich core and a surface shell consisting of low cross-link density NIPAM chains which are carboxy-terminated. Such morphology is arisen exploiting the tendency of allylic monomers such as VAA to behave as chain transfer agents instead of propagating monomers in free radical environments [24]. This particular structure allows VAA-microgels to ionize over a narrow pH range and exhibits large increases in

volume upon ionization. Such a microstructure provides both the sharp thermal sensitivity (NIPAM-rich core) and sharp pH sensitivity desirable for triggering and bioconjugation-related application.

1.3 SWELLING PROCESS OF PNIPAM BASED MICROGELS

The behavior of any polymer in a solvent is related to the balance between solvent-solvent, solvent-polymer and polymer-polymer interactions. For the case of PNIPAM in water, the polymer hydrogel bonds are related to water through the amide side chains. However, isopropyl groups on the side chains induce hydrophobic structuring of the water. This structured water leads to entropically driven polymer-polymer interactions caused by the hydrophobic effect [5]. Under conditions where PNIPAM has a random-coil structure, the solvent-polymer interactions are stronger than the polymer-polymer interactions. At higher temperatures, the hydrogen bonds to the water molecules break and there is an entropically favored release of bound and structured water, leading to the formation of a globular polymer conformation. In this case the polymer-polymer hydrophobic interactions become stronger than the polymer-solvent interactions, and the polymer phase separates. The temperature at which this phase separation occurs is the LCST.

Significant effort has been invested in predicting the swelling behavior of hydrogel systems. The most widely use of these approaches is the Flory-Huggins thermodynamic theory [25], which treats the swelling in terms of a series of osmotic pressure effects: the mixing of the polymer chains with the solvent, the elastic resistance of the cross-linked network to expansion or shrinking and the Donnan equilibrium of mobile counterions within the gel network.

The first to apply semi-empirical extended Flory-Huggins theory to predict the volume phase transitions of PNIPAM microgels was Prausnitz` group [26]. Some of the model parameters were obtained from the experimental properties of linear PNIPAM solutions. The predicted VPTT was about 1°C higher than the LCST of linear PNIPAM. However, the swelling predictions were significantly less accurate than those achieved with smaller, more homogeneous particles [27].

Flory-Huggins theory has been remarkably successful in describing the swelling of a wide range of bulk. This success is facilitated by the fact that bulk hydrogels can be considered as largely homogeneous on the microscale, with any microscopic inhomogeneous averaged out over the macroscale dimensions of the gel. Microgels, however, exhibit systematic inhomogeneities within their nanoscale dimensions. Strong, systematic trends in radial cross-linking density [28, 29] and functional group density [18, 19, 30] have been observed in PNIPAM-based microgel systems. Given the critical importance of the cross-link density to the elastic contribution to gel swelling and the functional group density to the charge contribution to gel swelling, such nanoscale gradients may have very significant effects on the swelling responses. Chain stiffness and direct charge-charge repulsion between the fixed network charges cannot be addressed using the basic Flory-Huggins model.

Combining the polyelectrolyte gel swelling theory of Hasa [31] with the direct polyelectrolyte repulsion term derived by Katchalsky and Michaeli [32], Hoare and Pelton [33] has published an approach which generalizes and describes the pH dependence of copolymer PNIPAM microgels containing carboxylic groups (COOH groups). This analysis takes into account the electrostatic interactions between the fixed charges within the polyelectrolyte (repulsive, driving swelling) and the salt counterions and the polyelectrolyte (attractive, driving deswelling).

1.4 BIOMEDICAL APPLICATIONS OF PNIPAM MICROGELS

Hydrogels are now widely used as biomaterials. These materials are biocompatible because their physicochemical properties are similar to those of the living tissues, *e. g.*, high water content, soft and rubbery consistency, and low interfacial tension with water or biological fluids. In addition, many hydrogels can alter their swelling degree in response to changes in their environment, such as pH, temperature, or ionic strength. Therefore hydrogels have found many applications in biomedicine and biotechnology, including tissue engineering scaffolds, biosensor, biomedical devices, and drug carriers [34, 35, 36].

Microgels are miniature hydrogels with a size ranging from tens of nanometers to several microns [37, 38]. Similar to bulky gels, microgels are usually biocompatible [39], and, due to their small size, they exhibit many advantages over bulky gels when used as biomaterials. One major advantage is that rate of the microgel responding to external stimuli is much faster than bulky gels [40, 41], as the rate of volume change is scaled as l^2 , where l is the relevant length scale of gel [42]. Secondly, colloidal microgel particles allow for minimally invasive administration when used as drug carriers.

Because of unique PNIPAM microgels properties, such as the size particles tunability, the thermo-responsivity, and the possibility to extend their sensitivity to other stimuli, they have found numerous applications, especially in biomedical areas. In particular PNIPAM microgels have been exploited for drug delivery and biosensing.

1.4.1 PNIPAM microgels for drug delivery

As drug carrier, PNIPAM microgels combine the advantages of both hydrogels and nanoparticles. The advantages, such as hydrophilicity,

flexibility, high water absorptivity, and good biocompatibility, are characteristic of hydrogels, while the advantages such as long life span in circulation and the possibility of being actively or passively targeted to the desired biophase, *e.g.* tumor sites, originate from their size which falls in the colloidal range. As recognition by the reticuloendothelial system is the principal reason for the removal of many colloidal drug carriers from the blood compartment [43], size of nanoparticle drug carriers should be controlled to be below 200 nm to extend their blood circulation time, which can be easily achieved for PNIPAM microgels.

PNIPAM microgel particles have a sponge-like structure with interstitial spaces filled with solvent. Usually the drug can be loaded by equilibrium partitioning between the solution and microgel phases [44]. Electrostatic interaction [44, 45], hydrophobic interaction [44], and hydrogen bonding [46] may play an important role for the drug loading. Drugs can also be loaded by the so called “breathing-in” method [47], in which the lyophilized microgels are resuspended in an aqueous solution of the drug. The payload can be completely imbibed by the hydrogel network, resulting in high loading efficiency. Similar to bulky gel carriers, the most common mechanism of drug release from PNIPAM microgel is passive diffusion [48]. The responsibility of PNIPAM microgels to various external stimuli, *e.g.*, temperature [49], pH [50], light [51], and glucose [52], has been widely exploited to achieve controlled drug release.

PNIPAM microgels have been tested for the controlled release of anticancer drugs [50, 52]. Their small size (below 200 nm) allows for the optimal extravasation into tumors. The drug can be incorporated by either physical means or covalent attachment. Numerous release mechanisms, which may be induced by biological stimuli such as a change in pH or interactions with enzymes, ions, or proteins, are available for the design of a controlled release system.

The presence of various surface functional groups allows for conjugation with targeting species, leading to targeted delivery of the drug to specified sites [47, 53]. For example, Nayak [17] synthesized a core-shell PNIPAM microgel with a fluorescently labelled core, which enables particle tracking, and a shell conjugated with folic acid, a targeting ligand. Both the folate-conjugated microgel and the non-conjugated control microgel were incubated with KB cells with overexpressed folate receptors. Only the folate-conjugated particles are internalized by the cells, revealing their potential specific targeting of cancer cells.

Through rational design, Das synthesized a pH-responsive PNIPAM microgel to delivery anti-cancer drugs to cancer cells [50]. The microgel size was controlled to be small (~150 nm), which maximizes extravasation into tumors. Receptor-specific ligand (transferrin) was conjugated onto the microgel surface for targeting the diseased cells. Drugs were loaded by physical means (*via* electrostatic interaction), instead of covalent attachment, which may potentially alter the drug's effectiveness. A release mechanism, which is triggered by biological stimuli, *i.e.*, pH change from 7.4 in the extracellular matrix to 4.5 in lysosome, was selected. An *in vitro* study reveals that the bio-functionalized, pH-responsive microgels can selectively carry the chemotherapeutic agent into tumor cells and cause significant cytotoxicity.

PNIPAM microgels are also good carrier for protein/peptide drugs. As a particulate drug carrier, microgels may protect the drugs from enzymatic degradation. High stability is one advantage of PNIPAM microgels over other particulate carriers, such as liposome or micelle. Particulate carriers from hydrophobic polymers may cause denaturation of protein drugs. In contrast, the PNIPAM microgel is hydrophilic, thus avoids this problem.

It is well-known that insulin should be supplied according to the blood glucose level of the patient. To achieve this, Zhang and others authors [52, 54, 55], synthesized glucose-sensitive poly(*N*-isopropylacryamide-co-3-

acrylamidophenylboronic acid) (P(NIPAM-AAPBA)) microgels using phenylboronic acid (PBA) group as glucose-sensing moiety. Glucose can bind with PBA and transfer it from a neutral, hydrophobic form to a negatively charged, hydrophilic form, which results in swelling of the PBA containing microgels. Two approaches have been used to synthesize P(NIPAM-AAPBA) microgels. The first one directly copolymerizes NIPAM and AAPBA [54, 56], while the second one introduces the functional groups by modification of a precursor poly(*N*-isopropylacrylamide-co-acrylic acid) (P(NIPAM-AAc)) microgel [52, 55]. The first approach doesn't seem very successful, as the glucose-responsibility of the resultant microgel strongly depends on its initial state, which depends itself on the initial temperature and the functionalization degree of the particle. It was postulated that the microgel might have an "island/ocean"-like heterogenous microstructure with PBA-rich domains as the "islands" and PNIPAM segments as the "ocean" [56], which results in the complicated behavior. In contrast, microgel synthesized *via* the second approach shows excellent glucose-sensitivity. At [Glu] = 0.01M, the hydrodynamic radius of the microgel increases one-fold, which correspond to a seven-fold increase in volume [52]. The high glucose sensitivity may be attributed to the relatively homogenous structure of the microgel, which it inherits from the P(NIPAM-AAc) precursor microgel [57].

Control over the permeability of a drug diffusing from the interior to the outside of microgels is key for their application as controlled drug delivery systems. For self-regulated insulin delivery, the permeability of the microgels should be able to be tuned by glucose. To demonstrate this, a core-shell microgel was designed in which the core can be degraded by NaIO₄, while the P(NIPAM-AAPBA) shell is glucose-sensitive [58]. The polymer debris from the degradation of the core diffuses out through the shell, which can be traced conveniently by turbidity. It was found that the polymer debris can be held by the P(NIPAM-AAPBA) nanoshell because of its low permeability, while they diffuse freely through a P(NIPAM-AA) shell. The permeability of

P(NIPAM-AAPBA) nanoshell can be tuned by temperature and pH, but more importantly by glucose. An increase in glucose concentration increases the swelling degree of the shell, thus its permeability, which in turn allows more polymer debris to be released. If insulin is loaded in the core area, it is expected that its release rate will increase with increasing glucose sensitive P(NIPAM-AAPBA) microgels were studied using a microgel monolayer as the platform [59]. It was found that the drug release at low temperature can be described as passive diffusion of the drugs, while at temperatures higher than VPTT, the drugs are released via a “squeeze-out” mechanism Figure 1.3. There glucose enhances the release of insulin at low temperature, but retards it at high temperature. However, drugs can bind with PBA groups through reversible phenylboronate ester bonds and glucose enhances their release at all temperatures. Therefore there may be two ways to achieve self-regulated insulin release. One is the modification of insulin with diol structures, so it can bind with PBA groups and glucose will enhance its release by competing for PBA binding site. A second way is to create a core-shell structure [58, 60, 61], in which the drug is loaded in the core, while the glucose-sensitive shell will control the release of the drug, as we suggested previously [58].

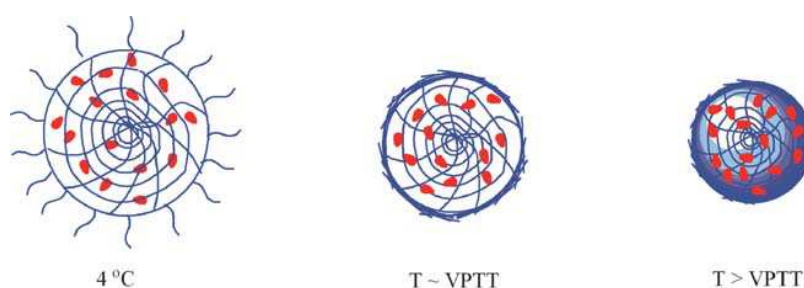


Figure 1.3: *Drug release mechanisms at different temperature. At 4 C°, the drug release follows a passive diffusion mechanism. At temperature close to the VPTT of the microgel, the diffusion of the drug is retarded by a thin dense “skin layer”. At temperature higher than the VPTT, the drugs are squeezed out due to the quick shrinkage of the microgel.*

1.4.2 PNIPAM microgels for biosensing

PNIPAM microgel particles offer good platforms for biosensing because of their large surface area, narrow size distribution and the versatility of functional groups on the surface. As an example, Ali [62] achieved DNA manipulation on a PNIPAM microgel surface. As shown in Figure 1.4, a 5'-amine modified DNA oligonucleotide (DNA1) was first coupled onto the microgel using EDC chemistry. Then the coupled DNA1 was ligated with a second DNA oligonucleotide (DNA2) in the presence of T4 DNA ligase and a template oligonucleotide. Rolling circle amplification (RCA) was carried out for signal amplification. Finally hybridization with a fluorescent DNA probe (DNA3) allows signal detection. Paper strips immobilized with DNA oligonucleotide modified microgels were further developed, which can be used to perform ligation/RCA-mediated amplification procedures for sensitive detection of DNA [63]. These DNA sensors have great promise in the identification of biological sources, such as specific pathogens.

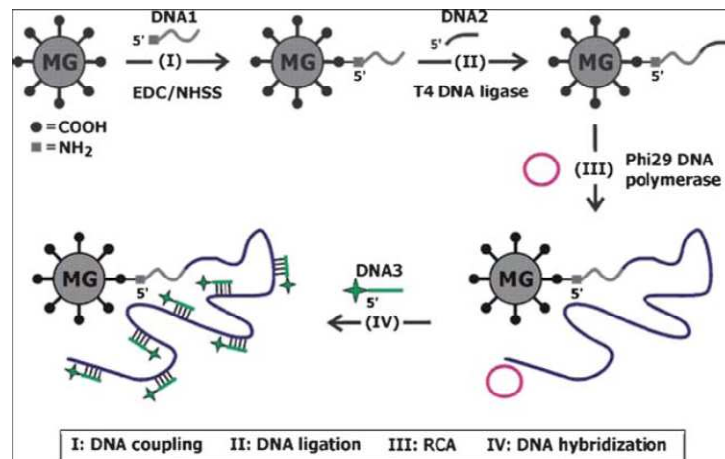


Figure 1.4: Schematic illustration of DNA manipulations on the PNIPAM microgel. (I) Covalent coupling of DNA with microgel by EDC/NHSS; (II) DNA ligation; (III) RCA; (IV) signal generation by hybridization with a fluorescent DNA probe.

In the above examples, PNIPAM microgels only act as a platform. The most prominent property of the PNIPAM microgel is its sensitivity to external stimuli. Sensors can be designed if this property is coupled with a suitable reporting method. Compared with sensors based on bulky hydrogels, the microgel-based sensors have the benefit that they respond much quicker.

Based on the glucose-sensitivity of PBA-functionized microgel, Wu [64] designed an optical glucose-sensor using fluorescent quantum dots (QDs) as optical labels. As shown in Figure 1.5, the fluorescent CdS QDs were synthesized *in situ* in the interior of the copolymer microgels. The resultant hybrid microgel remains glucose sensitive, *i.e.*, it swells to a larger degree in the presence of glucose. The swelling of the microgel results in an increase in the number of emission quenching centers located on the polymer–CdS QD interface, which in turn results in the quenching of the fluorescence of the CdS QDs. Therefore the optical detection of glucose can be achieved from the glucose induced fluorescence quenching. This sensor was further improved by using a PBA with a low pKa [65]. As a result, the sensor can detect glucose at physiological pH.

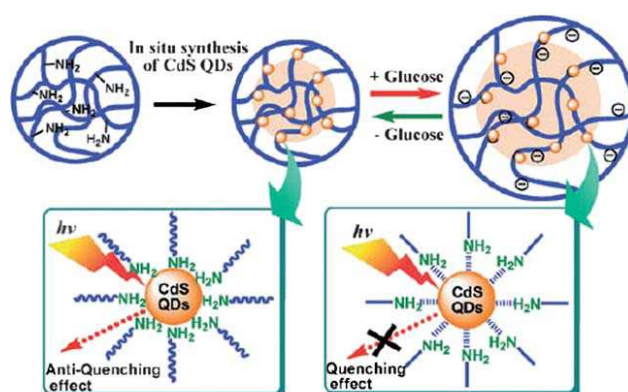


Figure 1.5: Reversible fluorescence quenching and anti-quenching of CdS QDs embedded in interior of glucose sensitive microgels in response to the change in glucose concentration.

REFERENCES

- [1] WO Baker. Microgel, a new macromolecule. relation to sol and gel as structural elements of synthetic rubber. *Rubber Chemistry and Technology*, 22(4):935–955, 1949.
- [2] Robert Pelton. Temperature-sensitive aqueous microgels. *Advances in Colloid and Interface Science*, 85(1):1 – 33, 2000.
- [3] R.H. Pelton and P. Chibante. Preparation of aqueous latices with n-isopropylacrylamide. *Colloids and Surfaces*, 20(3):247 – 256, 1986.
- [4] M. Heskins and J.E. Guillet. Solution properties of poly(n-isopropylacrylamide). *Journal of Macromolecular Science: Part A - Chemistry*, 2(8):1441–1455, 1968.
- [5] HG Schild. Poly (n-isopropylacrylamide): experiment, theory and application. *Progress in Polymer Science*, 17(2):163–249, 1992.
- [6] Mitsuhiro Shibayama and Toyochi Tanaka. Volume phase transition and related phenomena of polymer gels. In *Responsive gels: volume transitions I*, pages 1–62. Springer, 1993.
- [7] H.Y. Liu and X.X. Zhu. Lower critical solution temperatures of n-substituted acrylamide copolymers in aqueous solutions. *Polymer*, 40(25):6985 – 6990, 1999.
- [8] Yoshihito Osada and Simon B Ross-Murphy. Intelligent gels. *Scientific American*, 268:82–87, 1993.
- [9] Igor Yu Galaev. *'Smart' polymers in biotechnology and medicine*, volume 64. IOP Publishing, 1995.
- [10] Ron Dagani. Intelligent gels. *Chemical & engineering news*, 75(23), 1997.
- [11] Vanessa Castro Lopez, S.L. Raghavan, and M.J. Snowden. Colloidal microgels as transdermal delivery systems. *Reactive and Functional Polymers*, 58(3):175 – 185, 2004.
- [12] V.J Cornelius, M.J Snowden, J Silver, and G.R Fern. A study of the binding of the biologically important hematin molecule to a novel imidazole containing poly(n-isopropylacrylamide) microgel. *Reactive and Functional Polymers*, 58(3):165 – 173, 2004.
- [13] Gerald Gerlach, Margarita Guenther, Gunnar Suchaneck, Joerg Sorber, Karl-Friedrich Arndt, and Andreas Richter. Application of sensitive hydrogels in chemical and ph sensors. *Macromolecular Symposia*, 210(1):403–410, 2004.
- [14] Mikael Rasmusson and Brian Vincent. Flocculation of microgel particles. *Reactive and Functional Polymers*, 58(3):203 – 211, 2004.
- [15] Mark Mielke and Ralf Zimehl. Properties of differently charged poly(n-isopropylacrylamide) latex dispersions in alcohol-water mixtures. *Berichte der Bunsengesellschaft fur physikalische Chemie*, 102(11):1698–1704, 1998.

- [16] Akira Mamada, Toyochi Tanaka, Dawan Kungwachakun, and Masahiro Irie. Photoinduced phase transition of gels. *Macromolecules*, 23(5):1517–1519, 1990.
- [17] Satish Nayak and L. Andrew Lyon. Ligand-functionalized core/shell microgels with permselective shells. *Angewandte Chemie International Edition*, 43(48):6706–6709, 2004.
- [18] Todd Hoare and Robert Pelton. Highly pH and temperature responsive microgels functionalized with vinylacetic acid. *Macromolecules*, 37(7):2544–2550, 2004.
- [19] Shuiqin Zhou and Benjamin Chu. Synthesis and volume phase transition of poly(methacrylic acid-co-n-isopropylacrylamide) microgel particles in water. *The Journal of Physical Chemistry B*, 102(8):1364–1371, 1998.
- [20] Hironori Suzuki, Benlian Wang, Ryo Yoshida, and Etsuo Kokufuta. Potentiometric titration behaviors of a polymer and gel consisting of n-isopropylacrylamide and acrylic acid. *Langmuir*, 15(12):4283–4288, 1999.
- [21] Shoji Ito, Kazuyoshi Ogawa, Hironori Suzuki, Benlian Wang, Ryo Yoshida, and Etsuo Kokufuta. Preparation of thermosensitive submicrometer gel particles with anionic and cationic charges. *Langmuir*, 15(12):4289–4294, 1999.
- [22] Wei Xue, Simon Champ, and Malcolm B. Huglin. Observations on some copolymerisations involving n-isopropylacrylamide. *Polymer*, 41(20):7575 – 7581, 2000.
- [23] Herbert Morawetz. *Macromolecules in solution*. Wiley New York, 1975.
- [24] Calvin Everett Schildknecht. *Allyl compounds and their polymers (including polyolefins)*, volume 28. Wiley-interscience New York, 1973.
- [25] Flory and P J. *Principles of polymer chemistry*. Cornell University Press, 1953.
- [26] Toshiaki Hino and John M. Prausnitz. Swelling equilibria for heterogeneous polyacrylamide gels. *Journal of Applied Polymer Science*, 62(10):1635–1640, 1996.
- [27] Lise Arleth, Xiaohu Xia, Rex P. Hjelm, Jianzhong Wu, and Zhibing Hu. Volume transition and internal structures of small poly(n-isopropylacrylamide) microgels. *Journal of Polymer Science Part B: Polymer Physics*, 43(7):849–860, 2005.
- [28] Imre Varga, Tibor Gilanyi, Robert Meszaros, Genoveva Filipcsei, and Miklos Zrinyi. Effect of cross-link density on the internal structure of poly (n-isopropylacrylamide) microgels. *The Journal of Physical Chemistry B*, 105(38):9071–9076, 2001.
- [29] Ingo Berndt, Jan Skov Pedersen, Peter Lindner, and Walter Richtering. Influence of shell thickness and cross-link density on the structure of temperature-sensitive poly-n-isopropylacrylamide/poly-n-isopropylmethacrylamide core-shell microgels investigated by small-angle neutron scattering. *Langmuir*, 22(1):459–468, 2006. PMID: 16378460.

- [30] Karl Kratz, Thomas Hellweg, and Wolfgang Eimer. Influence of charge density on the swelling of colloidal poly(n-isopropylacrylamide-co-acrylic acid) microgels. *Colloids and Surfaces A: Physicochemical and Engineering Aspects*, 170(23):137 – 149, 2000.
- [31] J. Hasa, M. Ilavsky, and K. Dusek. Deformational, swelling, and potentiometric behavior of ionized poly(methacrylic acid) gels. i. theory. *Journal of Polymer Science: Polymer Physics Edition*, 13(2):253–262, 1975.
- [32] A. Katchalsky and I. Michaeli. Polyelectrolyte gels in salt solutions. *Journal of Polymer Science*, 15(79):69–86, 1955.
- [33] Todd Hoare and Robert Pelton. Functionalized microgel swelling: Comparing theory and experiment. *The Journal of Physical Chemistry B*, 111(41):11895–11906, 2007. PMID: 17894483.
- [34] Joseph Jagur-Grodzinski. Polymeric gels and hydrogels for biomedical and pharmaceutical applications. *Polymers for Advanced Technologies*, 21(1):27–47, 2010.
- [35] Allan S Hoffman. Hydrogels for biomedical applications. *Advanced Drug Delivery Reviews*, 54(1):3 – 12, 2002. Recent Developments in Hydrogels.
- [36] Todd R. Hoare and Daniel S. Kohane. Hydrogels in drug delivery: Progress and challenges. *Polymer*, 49(8):1993 – 2007, 2008.
- [37] Brian R. Saunders and Brian Vincent. Microgel particles as model colloids: theory, properties and applications. *Advances in Colloid and Interface Science*, 80(1):1 – 25, 1999.
- [38] Matthias Karg and Thomas Hellweg. New smart poly(nipam) microgels and nanoparticle microgel hybrids: Properties and advances in characterisation. *Current Opinion in Colloid & Interface Science*, 14(6):438 – 450, 2009.
- [39] H Weng, J Zhou, LP Tang, and ZB Hu. J. biomaterials sci. *Polymer Ed*, 15:1167–1180, 2004.
- [40] Jianping Wang, Daoji Gan, L. Andrew Lyon, and Mostafa A. El-Sayed. Temperature-jump investigations of the kinetics of hydrogel nanoparticle volume phase transitions. *Journal of the American Chemical Society*, 123(45):11284–11289, 2001.
- [41] Chad E. Reese, Alexander V. Mikhonin, Marta Kamenjicki, Alexander Tikhonov, and Sanford A. Asher. Nanogel nanosecond photonic crystal optical switching. *Journal of the American Chemical Society*, 126(5):1493–1496, 2004. PMID: 14759207.
- [42] Toyochi Tanaka and David J. Fillmore. Kinetics of swelling of gels. *The Journal of Chemical Physics*, 70(3):1214–1218, 1979.
- [43] Frank Alexis, Eric Pridgen, Linda K. Molnar, and Omid C. Farokhzad. Factors affecting the clearance and biodistribution of polymeric nanoparticles. *Molecular Pharmaceutics*, 5(4):505–515, 2008. PMID: 18672949.

- [44] Todd Hoare and Robert Pelton. Impact of microgel morphology on functionalized microgels for drug interactions. *Langmuir*, 24(3):1005–1012, 2008. PMID: 18179266.
- [45] Helena Bysell, Per Hansson, and Martin Malmsten. Effect of charge density on the interaction between cationic peptides and oppositely charged microgels. *The Journal of Physical Chemistry B*, 114(21):7207–7215, 2010. PMID: 20459071.
- [46] Ainara Imaz and Jacqueline Forcada. N-vinylcaprolactam-based microgels for biomedical applications. *Journal of Polymer Science Part A: Polymer Chemistry*, 48(5):1173–1181, 2010.
- [47] William H. Blackburn, Erin B. Dickerson, Michael H. Smith, John F. McDonald, and L. Andrew Lyon. Peptide-functionalized nanogels for targeted siRNA delivery. *Bioconjugate Chemistry*, 20(5):960–968, 2009. PMID: 19341276.
- [48] Mehrdad Hamidi, Amir Azadi, and Pedram Rafiei. Hydrogel nanoparticles in drug delivery. *Advanced Drug Delivery Reviews*, 60(15):1638 – 1649, 2008. 2008 Editors' Collection.
- [49] Christine M. Nolan, Leslie T. Gelbaum, and L. Andrew Lyon. 1h nmr investigation of thermally triggered insulin release from poly(n-isopropylacrylamide) microgels. *Biomacromolecules*, 7(10):2918–2922, 2006.
- [50] M. Das, S. Mardyani, W. Chan, and E. Kumacheva. Biofunctionalized pH-responsive microgels for cancer cell targeting: Rational design. *Advanced Materials*, 18(1):80–83, 2006.
- [51] Mallika Das, Nicolas Sanson, Daniele Fava, and Eugenia Kumacheva. Microgels loaded with gold nanorods: Photothermally triggered volume transitions under physiological conditions. *Langmuir*, 23(1):196–201, 2007. PMID: 17190504.
- [52] Yongjun Zhang, Ying Guan, and Shuiqin Zhou. Synthesis and volume phase transitions of glucose-sensitive microgels. *Biomacromolecules*, 7(11):3196–3201, 2006.
- [53] Erin B Dickerson, William H Blackburn, Michael H Smith, Laura B Kapa, L Andrew Lyon, and John F McDonald. Chemosensitization of cancer cells by siRNA using targeted nanogel delivery. *BMC cancer*, 10(1):10, 2010.
- [54] Veronique Lapeyre, Isabelle Gosse, Sylviane Chevreux, and Valerie Ravaine. Monodispersed glucose-responsive microgels operating at physiological salinity. *Biomacromolecules*, 7(12):3356–3363, 2006.
- [55] Todd Hoare and Robert Pelton. Engineering glucose swelling responses in poly(n-isopropylacrylamide)-based microgels. *Macromolecules*, 40(3):670–678, 2007.
- [56] Hui Ge, Yanwei Ding, Chengcheng Ma, and Guangzhao Zhang. Temperature-controlled release of diols from n-isopropylacrylamide-co-acrylamidophenylboronic acid microgels. *The Journal of Physical Chemistry B*, 110(41):20635–20639, 2006.
- [57] Yapeng Zhang, Kun Liu, Ying Guan, and Yongjun Zhang. Assembling of gold nanorods on p(nipam-aapba) microgels: a large shift in the plasmon band and colorimetric glucose sensing. *RSC Adv.*, 2:4768–4776, 2012.

- [58] Yongjun Zhang, Ying Guan, and Shuiqin Zhou. Permeability control of glucose-sensitive nanoshells. *Biomacromolecules*, 8(12):3842–3847, 2007.
- [59] Pengxiao Liu, Qiaofang Luo, Ying Guan, and Yongjun Zhang. Drug release kinetics from monolayer films of glucose-sensitive microgel. *Polymer*, 51(12):2668 – 2675, 2010.
- [60] Qiaofang Luo, Pengxiao Liu, Ying Guan, and Yongjun Zhang. Thermally induced phase transition of glucose-sensitive core-shell microgels. *ACS Applied Materials & Interfaces*, 2(3):760–767, 2010. PMID: 20356278.
- [61] Veronique Lapeyre, Christophe Ancla, Bogdan Catargi, and Valerie Ravaine. Glucose-responsive microgels with a core-shell structure. *Journal of Colloid and Interface Science*, 327(2):316 – 323, 2008.
- [62] Md Monsur Ali, Shunxing Su, Carlos D. M. Filipe, Robert Pelton, and Yingfu Li. Enzymatic manipulations of dna oligonucleotides on microgel: towards development of dna-microgel bioassays. *Chem. Commun.*, pages 4459–4461, 2007.
- [63] M. Monsur Ali, Sergio D. Aguirre, Yaqin Xu, Carlos D. M. Filipe, Robert Pelton, and Yingfu Li. Detection of dna using bioactive paper strips. *Chem. Commun.*, pages 6640–6642, 2009.
- [64] Weitai Wu, Ting Zhou, Jing Shen, and Shuiqin Zhou. Optical detection of glucose by cds quantum dots immobilized in smart microgels. *Chem. Commun.*, pages 4390–4392, 2009.
- [65] Weitai Wu, Michael Aiello, Ting Zhou, Alexandra Berliner, Probal Banerjee, and Shuiqin Zhou. In-situ immobilization of quantum dots in polysaccharide-based nanogels for integration of optical ph-sensing, tumor cell imaging, and drug delivery. *Biomaterials*, 31(11):3023–3031, 2010.

CHAPTER II

Engineering tunable temperature and pH responsive PNIPAM-VAA core-shell microgel particles

INTRODUCTION

Sensitive microgels are colloiddally stable hydrogels responsive to external stimuli such as ionic strength [1], solvent composition [2], radiation [3], selective reaction [4] and pH [5]. PNIPAM is the most widely investigated temperature-sensitive microgel system, with particle sizes ranging from tens of nanometers up to micrometers. Generally, PNIPAM microgels have a LCST of 32 °C and, when chemically cross-linked in aqueous solution, show pronounced particle deswelling if heated above the VPTT [6]. PNIPAM microgels nowadays are present in a wide range of biomedical applications such as drug delivery [7], biomolecules immobilization and absorption [8] or sensor [9].

PNIPAM thermo-responsive microgels benefit from their capacity of being easily tuned to deswell. The possibility to tune the VPTT becomes important for potential applications that demand environmentally triggered changes in the microgel structure, surface charge and gel hydrophobicity. The tuning of the hydrophilic and hydrophobic groups ratio offers the possibility to modulate the VPTT of microgels [10]. This tunability can be achieved by using PNIPAM together with a copolymer containing carboxylic groups [5]

to encode the pH sensitivity in microgels. Indeed, carboxylic acid groups inside the microgels are ionized by increasing the pH, which causes an increase in the osmotic pressure inside the particle (due to the counter-ions) and shifts the VPTT of the microgel to higher solution temperatures.

Hoare and Pelton [11] introduced multi-responsive microgels of core-shell morphology based on PNIPAM functionalized with vinylacetic acid (VAA). Such morphology consists of a NIPAM-rich core and a surface shell made of low cross-link density NIPAM chains, which are carboxy-terminated. These features are due to the tendency of allylic monomers -such as VAA- to behave as chain transfer agents instead of propagating monomers in free radical environments [12]. The spatial separation of two different components -each responsive to a single stimulus- gives an important contribution to the modulation of responsivity. This particular structure allows VAA-PNIPAM microgels to ionize over a narrow pH range and to exhibit a large increase in volume upon ionization. It provides valuable features such as faster rates of swelling and a sharp thermal and pH sensitivity. The influence of the relative core-to-shell ratio implies an additional tuning factor for microgel responsive.

In this work highly monodisperse VAA-PNIPAM particle samples were prepared and the effect of changes in pH, temperature and core-to-shell ratio has been investigated by transmission electron microscopy (TEM) and scattering techniques. In particular, the particle swelling was followed by neutron and light scattering techniques during alkalization. The non-uniform swelling resulting from small angle neutron scattering (SANS) and static light scattering (SLS) was interpreted in terms of a core-shell model, consolidating the structure proposed by Hoare and Pelton [11]. The studied VAA-PNIPAM particle resulted composed of a NIPAM-rich core, whose volume varies according to the PNIPAM LCST, and most of the VAA groups localized in the shell, whose volume varies depending on the relative alkalization. When the pH is lower than the $pK_a \approx 4.8$ of VAA, all the acid

groups are non-ionized and the shell shrinks. Above the pK_a , the shell is fully swollen and microgels exhibit a phase transition shifting, which depends on the pH value and on the relative size of core to shell. As a consequence, the control of the microgel structure becomes fundamental to modulate how the acid shell thickness influences the microgel responsivity. Form factor analysis indicates that, by changing the mutual influence of core to shell, it is possible to modulate the sensitivity of the microgel to the environmental variations.

2.1 MATERIALS AND METHODS

2.1.1 Materials

N-Isopropylacrylamide (NIPAM, 97%), vinylacetic acid (VAA, 97%), *N,N'*-Methylenebisacrylamide (MBA, 99%) as cross-linker, potassium persulfate (KPS, 99%) as starter, and sodium dodecyl sulfate (SDS) were purchased from by Sigma-Aldrich and used as received. Water used in the synthesis and characterization was of Millipore Milli-Q grade.

2.1.2 Microgel Preparation

Two separated microgel samples were synthesized: VAA-SDS-CS and VAA-CS. The composition in terms of monomers and cross-linkers was equal, while differentiation in size was obtained during VAA-SDS-CS synthesis by SDS addition to get a smaller microgel size.

The microgel particles were synthesized with a standard precipitation polymerization method [11]. Polymerizations were carried out in a 200 ml three-necked flask equipped with a condenser and a stirrer. NIPAM (1.4 g), MBA (0.07 g), SDS (0.05 g), and the functional monomer VAA (0.07 g) were all dissolved in 50 ml of water and heated to the polymerization temperature of 70 °C under a nitrogen purge. After 30 min. 5 ml of initiator solution (KPS) were injected to initiate the polymerization, which were carried out for 5 hours. After cooling, all microgels were cleaned by dialyzing against pure water for 15 days. The microgels were stored at 4 °C at a concentration $c \approx 2.5$ wt%.

2.1.3 TEM micrographs

A solution of VAA-CS at a concentration $c \approx 0.5$ wt% was prepared. The anionic functional groups in the microgel were selectively stained by mixing a 0.05 ml aliquot of the microgel suspension with 0.5 ml of a 1 mM uranyl acetate solution and stirring the mixture for 1 h. A single drop of the stained suspension was dropped on a Formvar-coated copper TEM grid and dried overnight. TEM micrographs were acquired at 200 kV (FEI Company – TECNAI G2 20, Hillsboro, USA).

2.1.4 Light Scattering experiments

The apparatus used to perform the dynamic and static light scattering (DLS/SLS) experiments was a compact goniometer (ALV-LASER GmbH – ALV/CGS-3, Langen, Germany) operating at a wavelength of 633nm in vacuum and a time correlator (ALV-LASER GmbH – ALV/LSE-5003, Langen, Germany) to perform the DLS experiments. Each sample was

measured in highly diluted and temperature stable conditions ($c \approx 0.01$ wt%). The sample temperature was controlled by an external heating and refrigerated bath (JULABO – FS18, Seelbach, Germany). The pH value was adjusted the day before the measurement with HCl or NaOH, respectively, and controlled with a pH-meter (METTLER TOLEDO – Seven easy, Columbus, USA) directly before each measurement. The scattering angle θ , was varied from 20° to 140° .

2.1.5 Dynamic Light Scattering Analysis

The hydrodynamic radii, R_h , of the particles were determined by fitting the long-time baseline of the intensity correlation function [13]. The used formula is a derivate of the moment-based expression from Pusey and Van Megen [14] and the Siegert relation [15] for the field-field time autocorrelation function, and is written as:

$$g^{(2)} = B + \beta \exp(-2\bar{\Gamma}\tau) \left(1 + \frac{\mu_2}{2!} \tau^2\right)^2 \quad (1),$$

where the factor B is referred to the baseline, β the factor of the experimental geometry, and τ the delay time of the normalized autocorrelation function of the scattered light intensity. For monodisperse particles in solution the field-correlation function decays exponentially with a decay rate $\bar{\Gamma} = Dq^2$, with the diffusion coefficient $D = k_B T / 6\pi\eta R_h$, where k_B is the Boltzmann constant, T the temperature, and η the dynamic viscosity of the Stokes-Einstein relation. R_h is the hydrodynamic radius of a sphere that would have the same average diffusion constant as the scattering particles [13]. The magnitude of the scattering wave vector $q = (4\pi n / \lambda_0) \sin(\theta/2)$, with n the refractive index of the solvent, and λ_0 the laser wavelength of the used goniometer.

2.1.6 Small Angle Neutron Scattering experiments

SANS experiments were performed on the instruments SANS-I and SANS-II at SINQ, Paul Scherrer Institut, Switzerland. With a radius close to 100 nm, the VAA-SDS-CS particles have a size that is relatively large for SANS. Therefore, the instruments were set up to reach low q values. On SANS-I, two setups were used: The sample-detector distance and the collimation distance were equal and were 18 m or 4.5 m; the wavelength was 8 Å. These two settings give access to the q range from 0.025 nm⁻¹ to 1.14 nm⁻¹. SANS-II is a smaller instrument, where also two different settings were used: The sample-detector and collimation distances were equal and chosen to be 6 m and 2 m with a wavelengths of 10.5 Å and 8 Å, respectively. These two settings give access to the q range from 0.023 nm⁻¹ to 1.1 nm⁻¹. The samples were suspended in D₂O to improve the scattering length density contrast and were measured in quartz cuvettes with a thickness of 2 mm.

2.1.7 Small Angle Neutron Scattering and Static Light Scattering

Analysis

Particle interactions can be neglected for sufficiently diluted colloidal dispersions or polymer solutions and scattering intensity can be described by the form factor $P(q)$. Two different form factors were used to fit the experimental data of pH and temperature sensitive VAA microgels.

It is well known that PNIPAM microgel structure is presumably composed by a uniformly cross-linked core and by a shell in which the polymer density decreases towards the surface of the particle [16]. The particle form factor for an inhomogeneous sphere $\tilde{P}_{\text{inho}}(q)$ can be modeled, in reciprocal space, as the product of the form factor of a homogeneous

sphere and a Gauss function with a characteristic length scale σ_{surf} proportional to the thickness of the shell [17, 18].

$$\tilde{P}_{\text{incho}}(q) = \left[\frac{3[\sin(qR_c) - qR_c \cos(qR_c)]}{(qR_c)^3} \exp\left(-\frac{(\sigma_{\text{surf}} q)^2}{2}\right) \right]^2 \quad (2),$$

Within this model, the polymer density decreases to half of its core value at the core radius R_c and reaches the overall particle size (core + shell) at $R_{\text{cs}} = R_c + 2\sigma_{\text{surf}}$.

For polymer particle composed by a core-shell structure, a different model is used, with a polymer density (Figure 2.1 b) defined as

$$\begin{aligned} \rho(r) &= 1 & 0 < r < R_c^* \\ \rho(r) &= \varphi_{\text{shell}} & R_c^* < r < R_{\text{cs}}^* \\ \rho(r) &= 0 & R_{\text{cs}}^* < r \end{aligned}$$

The particle core-shell form factor $\tilde{P}_{\text{cs}}(q)$ is differently calculated, given by:

$$\tilde{P}_{\text{cs}}(q) = \left[\frac{3\varphi_{\text{shell}}qR_{\text{cs}}^* \cos(qR_{\text{cs}}^*) - 3(-1 + \varphi_{\text{shell}})(qR_c^* \cos(qR_c^*) - \sin(qR_c^*)) - 3\varphi_{\text{shell}}\sin(qR_{\text{cs}}^*)}{q^3((-1 + \varphi_{\text{shell}})R_c^* - \varphi_{\text{shell}}R_{\text{cs}}^*)^3} \right]^2 \quad (3),$$

where R_c^* is the core radius and R_{cs}^* is the overall particle size.

In these two models, polydispersity has been included by assuming a Gaussian radius distribution by

$$W(\bar{R}, R, \sigma_{\text{poly}}) = \frac{1}{\sqrt{2\pi\sigma_{\text{poly}}^2\bar{R}^2}} \exp\left[-\frac{(R-\bar{R})^2}{2\pi\sigma_{\text{poly}}^2\bar{R}^2}\right] \quad (4),$$

where \bar{R} is the average particle radius and σ_{poly} denotes the relative particle size polydispersity. For simplicity \bar{R} is assumed to be R_c or R_{cs}^* , in order if it has been calculated using $\tilde{P}_{\text{incho}}(q)$, or $\tilde{P}_{\text{cs}}(q)$. The solution form factor for the whole solution is thus described by

$$P(q) = \int \tilde{P}(q) \cdot W(\bar{R}, R, \sigma_{\text{poly}}) \quad (5).$$

SANS can investigate higher q values than SLS, thus scattering intensity results also by the fluctuations of the network. To account for this contribution, a Lorentzian function $I_L = I_L(0) / [1 + q^2\xi^2]$ was added to the form factor model used to analyze the SANS data, where ξ can be considered related to the microgel mesh size [19, 20, 21, 22, 23, 24].

2.2 RESULTS AND DISCUSSION

2.2.1 Transmission electron micrographs

Core-shell microgels based on PNIPAM functionalized with VAA are characterized by a NIPAM-rich core and a surface shell consisting of low cross-link density NIPAM chains, which are carboxy-terminated. Two different samples VAA-SDS-CS and VAA-CS, expected to have the same morphological and structural properties were synthesized in this work. The swollen microgel structure for a pH level above the pK_a of VAA is illustrated in Figure 2.1a. The functional groups distribution of VAA-CS sample is shown in the TEM micrograph in Figure 2.1b, where the PNIPAM microgel structure with a uniformly cross-linked core and the corresponding shell in which the polymer density decreases towards the surface of the particle is illustrated. PNIPAM-VAA microgels present a core-shell structure, where the stained functional groups are localized on the surface. This particular distribution is mainly due to two factors: the behavior of VAA monomer as a chain transfer [12, 25], like all the allylic monomers; and the NIPAM monomer propagation rate, which is several orders of magnitude faster compared to VAA [12]. The first factor contributes to the production of single vinylacetic groups incorporated on the chain-ends of NIPAM, while the second factor causes the rich core of NIPAM to be formed before the VAA-containing oligomers are produced via chain transfer.

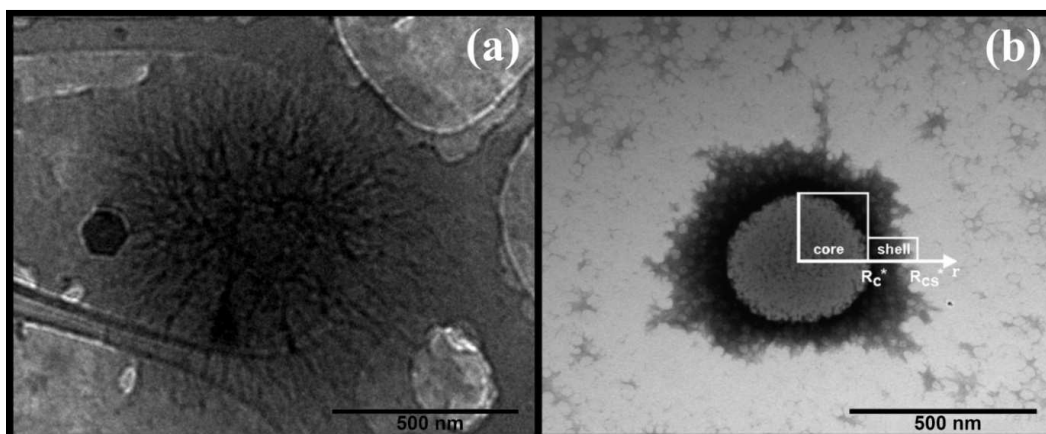


Figure 2.1: TEM micrograph of VAA-CS microgels. (a) Cryo-TEM of swollen microgels; (b) shrunken microgel with anionic sites, where the PNIPAM microgel structure with a uniformly cross-linked core and the corresponding shell in which the polymer density decreases towards the surface of the particle is illustrated. The sample illustrates a core-shell structure, where VAA groups are localized on the surface.

2.2.2 Hydrodynamic radii and swelling ratio

Both VAA-SDS-CS and VAA-CS particles are temperature and pH sensitive. The dependence of the swelling ratio on temperature is shown in Figure 2.2 for both samples at different pH values. Generally, VAA-SDS-CS and VAA-CS particles have different radii depending on pH, in particular -at 25 °C- the VAA-SDS-CS radius is measured to be 70 - 150 nm, while the VAA-CS radius is 450 - 600 nm.

Both samples present approximately the same swelling ratio values for equal pH levels, which ensure similar microgel structure and morphology. Generally, the swelling of the particle is strongly influenced by the presence of carboxylic groups. When pH levels increase, the repulsion between ionized acid groups becomes stronger, creating an osmotic pressure inside the particle that delays the shrinkage, resulting in a bigger particle size. In fact, in

the pH range of the pK_a of VAA, the VPTT is similar to the LCST of PNIPAM. Swelling profiles are rather sharp in terms of both the narrow temperature range of their volume phase transition and the degree of volumetric deswelling observed upon heating. Specifically, for pH 3 the VPTT is ~ 32 °C. By increasing the pH level above the pK_a of VAA, the size distribution of the measured particles increases and the VPTT shifts to higher temperatures. For pH 8, where most of the carboxylic groups are deprotonated, the VPTT shifts up to ~ 39 °C for VAA-SDS-CS and ~ 45 °C for VAA-CS, besides showing a broader swelling profile. Eventually, at high temperatures all the radii at all pH collapsed to one single size. At very low pH and high temperatures both samples tend to aggregate, because acid groups become fully protonated and repulsions is minimized, as the particles are in a collapsed state. This behavior limits scattering measurements for VAA-SDS-CS the pH 3 sample at temperatures under 30 °C.

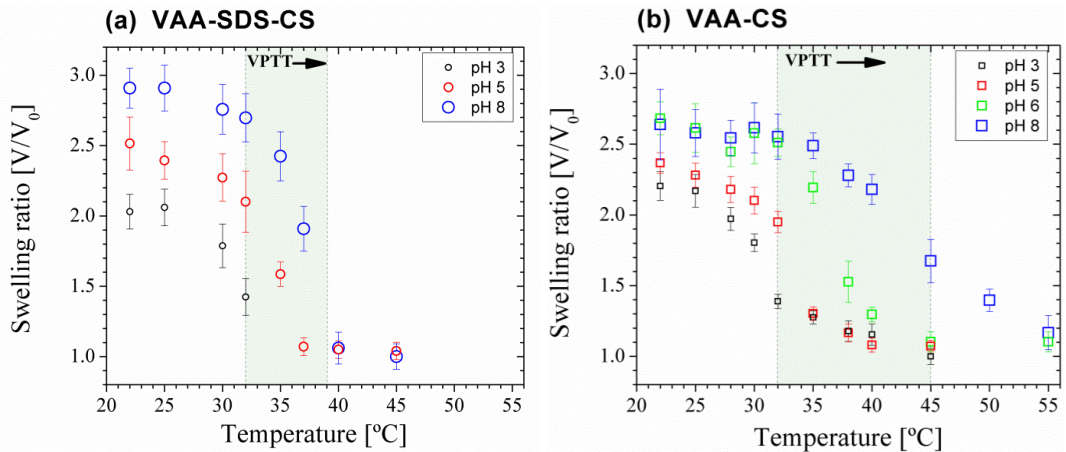
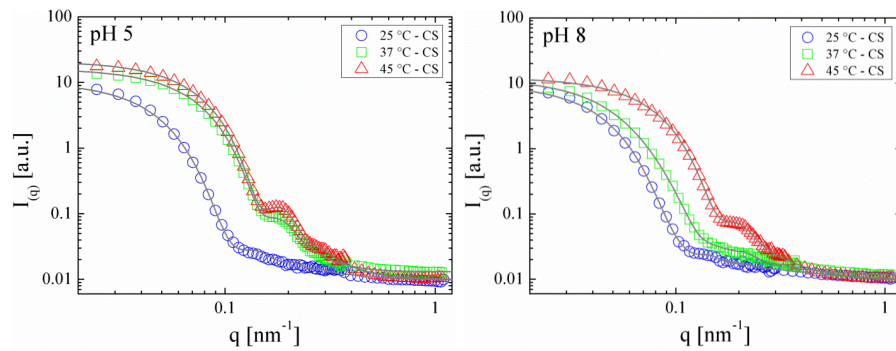


Figure 2.2: Swelling ratio of VAA-SDS-CS (a) and VAA-CS (b) at different pH values measured by DLS. At pH 3 the VPTT is ~ 32 °C and profiles are rather sharp. At higher pH values the particle size increases and the VPTT shifts. For high temperatures all radii at all pH values collapse into one single microgel size.

2.2.3 Structure of VAA-particles

The structure of microgel particles in solution is obtained by analyses of the form factor using SANS and SLS measurements. SANS and SLS data for pH 5 and pH 8, obtained from our core-shell particles at three different temperatures are shown with corresponding fits in Figure 2.3. The form factor minima indicate that polydispersity is small, with an average of $\sim 12\%$ (see Table 2.1 for SANS and Table 2.2 for SLS). A shift of the form factor minimum toward higher q values is observed with increasing temperature and decreasing pH because of the shrinking particle size.

(a) SANS –VAA-SDS-CS



(b) SLS - VAA-CS

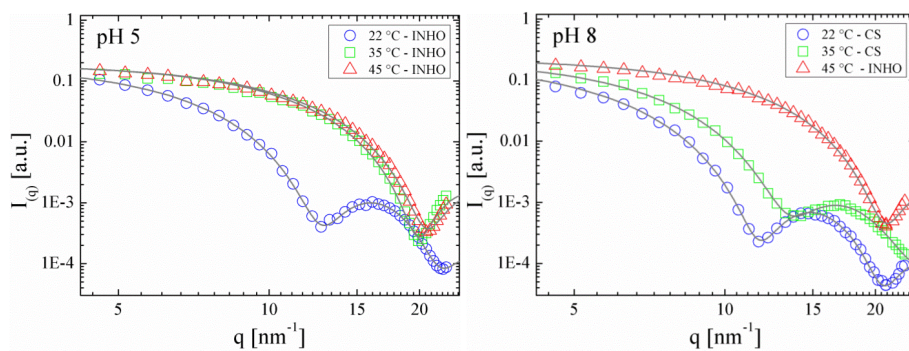


Figure 2.3: SANS (a) and SLS (b) scattering graphs at different temperatures for pH 5 and pH 8. The index INHO in the legend indicates the inhomogeneous form factor fit, while CS is used for the core-shell fit. All corresponding fitting curves are plotted as gray line.

2.2.4 Small Angle Neutron Scattering

We calculated the VAA-SDS-CS particle radius through the core-shell model. In Figure 2.4 core and shell radii are reported as function of temperature at two different pH values, pH 5 and pH 8. Microgel cores are pH independent, while shells vary with pH. At 25 °C, when microgel particles are fully swollen, R_c^* is about 30 nm. By increasing the temperature up to 37 °C, significantly above the PNIPAM LCST, R_c^* reaches the fully shrunken state of 21 nm and remain collapsed for any higher temperature. This effect is due to the high NIPAM concentration in the core. Otherwise, R_{cs}^* remains swollen for high pH and increasing temperature because of the VAA in the shell. R_{cs}^* of 53 nm for pH 5 and 59 nm for pH 8 was measured at 25 °C. Whereas by increasing the temperature up to 37 °C, the pH 5 shell collapse to R_{cs}^* of 33 nm, while pH 8 shells are still swollen. This behavior agrees with the swelling ratio values at 37 °C in Figure 2.2a, where pH 8 particles have not collapsed yet, while pH 5 particles are almost shrunken. Also the polymer density, ϕ_{shell} , confirms this behavior (see inset in Figure 2.4). The polymer distribution at 25 °C is equally distributed for both pH levels, while for 37 °C at pH 5 most of the shell polymers go into the core whereas shells are still swollen at pH 8.

In terms of LCST, a VPTT shift to higher temperature and pH values is recognized. This shift implies a change of the relative core-to-shell ratio, which can be used to modulate the microgel phase transition. Eventually, at 45 °C the pH 5 and pH 8 shells collapse and R_{cs}^* is 32 nm (see Table 2.1). The particle size from SANS measurements is in good agreement with the hydrodynamic radius.

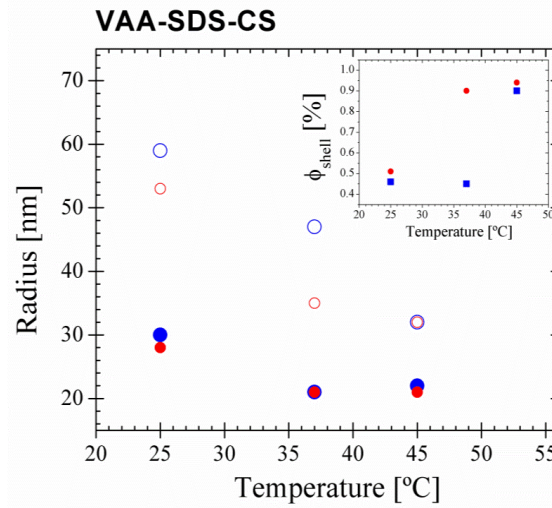


Figure 2.4: Radius of VAA-SDS-CS particles calculated from SANS measurements at pH 5 (red circles) and pH 8 (blue circles). Solid circles represent the pH-independent NIPAM-rich cores, R_c^* , while open circles give R_{cs}^* with the pH-dependent VAA shell structure. The inset shows the polymer density of the microgel shell as function of temperature at pH 5 (red circles) and pH 8 (blue squares).

Table 2.1. Summary of the structural parameters obtained from SANS data analysis.

pH	T	R_c^*	σ_{poly}^*	ϕ_{shell}^*	ξ	R_{cs}^*
	[°C]	[nm]	[%]	[%]	[nm]	[nm]
5	25	28	12	51	11	53
5	37	21	14	92	7	33
5	45	21	12	98	7	32
8	25	30	15	46	12	59
8	37	21	17	45	6	47
8	45	21	13	92	4	32

*refers to values obtained by core-shell form factor $P_{cs}(q)$ analyses.

2.2.5 Static light scattering

The inhomogeneous sphere model was used to fit SLS data for pH 3 and pH 5 and temperatures higher than 40 °C. Otherwise, the core-shell model was used (pH 6 and pH 8).

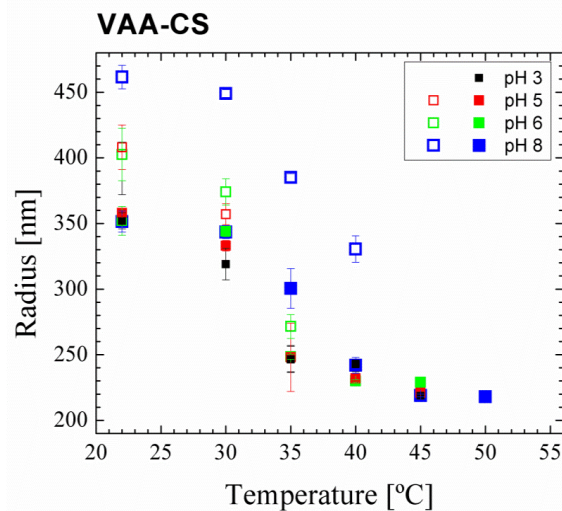


Figure 2.5: Radius of VAA-CS particles calculated from SLS measurements at different pH levels. Solid squares represent the pH-independent NIPAM-rich cores, R_c^* , while the open squares give the R_{cs}^* with the pH-dependent VAA shell structure.

In Figure 2.5 R_c^* and R_{cs}^* from SLS data analyses are reported as function of temperature at pH 3, 5, 6 and 8. As it was expected from SANS measurements, particles are composed of a mainly pH-independent core and a pH-dependent shell, implying a tunable microgel VPTT. For pH 3 cores, the VPTT is ~32 °C and increases until 35 °C for pH 8, indicating that only a small amount of VAA is localized in the core. At 22 °C the average R_c^* has been calculated with ~353 nm. When increasing the temperature up to 40 °C, R_c^* reach the shrunken state of about ~237 nm and remain collapsed at higher temperatures, apart from pH 8, whose size is slightly bigger.

Table 2.2. Summary of the structural microgel parameters obtained from SLS data analyses.

pH	T	R_c	σ_{poly}	φ_{shell}	ξ	R_{cs}
	[°C]	[nm]	[%]	[%]	[nm]	[nm]
3	22	352 ± 6	20 ± 7	6 ± 1	-	392 ± 20
	30	319 ± 12	0	11 ± 1	-	319 ± 12
	35	247 ± 10	0	6 ± 4	-	247 ± 10
	40	243 ± 3	0	7 ± 2	-	243 ± 3
	45	219 ± 2	0	7 ± 1	-	219 ± 2
5	22	358 ± 3	25 ± 7	8 ± 1	-	408 ± 17
	30	333 ± 4	12 ± 2	10 ± 1	-	357 ± 8
	35	248 ± 26	0	7 ± 3	-	248 ± 26
	40	232 ± 3	0	7 ± 1	-	232 ± 3
	45	221 ± 1	0	6 ± 1	-	221 ± 1
6	22	$352 \pm 11^*$	-	$13 \pm 2^*$	$42 \pm 3^*$	$402 \pm 20^*$
	30	$344 \pm 4^*$	-	$21 \pm 1^*$	$52 \pm 2^*$	$374 \pm 10^*$
	35	$248 \pm 2^*$	-	$5 \pm 1^*$	$69 \pm 3^*$	$271 \pm 9^*$
	40	230 ± 1	0	8 ± 1	-	230 ± 1
	45	229 ± 1	0	14 ± 1	-	229 ± 1
8	22	$351 \pm 8^*$	-	$14 \pm 1^*$	$43 \pm 4^*$	$461 \pm 9^*$
	30	$344 \pm 5^*$	-	$24 \pm 6^*$	$42 \pm 3^*$	$449 \pm 3^*$
	35	$300 \pm 15^*$	-	$11 \pm 1^*$	$62 \pm 6^*$	$385 \pm 3^*$
	40	$242 \pm 6^*$	-	15 ± 3	$64 \pm 7^*$	$331 \pm 10^*$
	45	219 ± 1	0	5 ± 1	-	219 ± 1
	50	218 ± 1	0	6 ± 1	-	218 ± 1

*refers to the values obtained by core-shell form factor $P_{\text{cs}}(q)$ analyses.

The VPTT changes according to pH levels. At 22 °C the microgel shells are swollen with R_{cs}^* of 400 nm and 476 nm at pH 6 and pH 8 are, respectively. By increasing the temperature up to 40 °C -where the core has reached the shrunken state- pH 6 shells collapse and pH 8 shells start shrinking. This

behavior agrees with values at 40 °C in Figure 2.2b, where pH 8 particles have not collapsed yet, while pH 6 particles are almost shrunken. At 45 °C all measured particles are collapsed, with a value comparable to the hydrodynamic radius size.

These results are in good agreement with literature [11], as shown in our TEM micrographs, where microgel particles are composed by a non-pH-sensitive core and a pH-sensitive shell. R_c^* depends mainly on temperature, implying high concentration of PNIPAM chains, while all the vinylic groups are concentrated in the pH-sensitive shell, affecting the shell thickness and the VPTT of the microgel particles

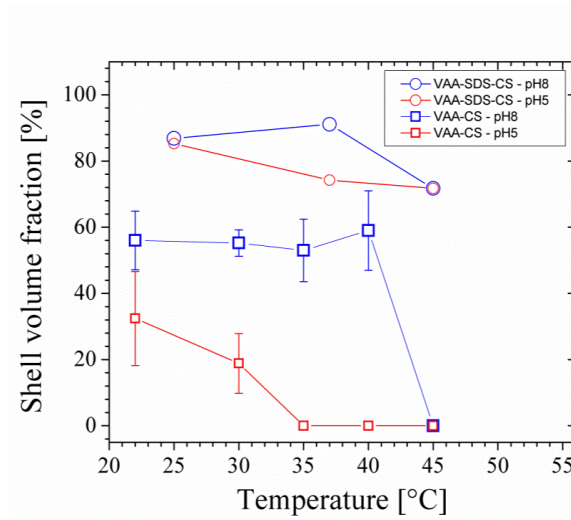


Figure 2.6: Shell volume fraction of VAA-CS and VAA-SDS-CS. The VAA-CS microgel shows a significant smaller shell volume fraction compared to VAA-SDS-CS at all temperature levels, until the microgel shells collapse at 45 °C.

A comparison of the core-to-shell ratio for both microgels (Figure 2.6) concludes the discussion. The shell volume fractions of VAA-CS microgel show significant smaller values compared to VAA-SDS-CS at all temperature levels. Moreover, an increased relative pH-dependence of VAA-SDS-CS from 25 °C to 37 °C compared to the other sample is recognized.

This indicates a different degree of deswelling between the two microgel types, according to the applied pH values, until the microgel shells collapse at 45 °C. Smaller sized microgels are highly responsive to external triggers due to their internal structure.

CONCLUSIONS

We tuned the PNIPAM-VAA microgel sensitivity in terms of VPTT features: position, width and induced degree of swelling. The swelling behavior of differently sized core-shell microgels depending on pH and temperature changes has been proofed by SANS and light scattering measurements. We were able to obtain a higher or lower degree of shell swelling by modulating the core-to-shell ratio via pH, particle size and temperature variations.

The result is a microgel composed of a NIPAM-rich core and a surface shell consisting of low cross-link density carboxy-terminated NIPAM chains, which collapse for pH values smaller than the pK_a of the VAA. Increasing the solution temperature, at pH levels above the pK_a , the core passes through a phase transition equal to the PNIPAM LCST, while the shell remains swollen at a degree that depending on the applied pH level. As a consequence of an increased pH value, the VPTT position and width of the microgel shifts to higher values, providing the possibility to tune VAA-PNIPAM microgel phase transition using external triggers. At temperatures above 40 °C all microgel shells collapse and no specific pH sensitivity can be observed.

The ability to independently tune the VPTT through the core-shell architecture increases the relevance of PNIPAM microgel. In fact, it can be used in applications that rely on switch on/off mechanisms of interaction between the microgel structure and the surrounding environment.

REFERENCES

- [1] Rasmusson, M.; Vincent, B. Flocculation of microgel particles. *React. Funct. Polym.* 2004, 58, 203-211.
- [2] Mielke, M.; Zimehl, R. Properties of differently charged poly(*N*-isopropylacrylamide) Latex dispersions in alcohol-water mixtures. *Ber. Bunsen-Ges.* 1998, 102, 1698-1704.
- [3] Mamada, A.; Tanaka, T.; Kungwachakun, D.; Irie, M. Photoinduced phase transition of gels. *Macromolecules (Washington, DC, U. S.)* 1990, 23, 1517-1519.
- [4] Nayak, S.; Lyon, L. A. Ligand-Functionalized Core/Shell Microgels with Permselective Shells. *Angew. Chem., Int. Ed.* 2004, 43, 6706-6709.
- [5] Hoare, T.; Pelton, R. Functionalized Microgel Swelling: Comparing Theory and Experiment. *J. Phys. Chem. B* 2007, 111, 11895-11906.
- [6] Schild, H. G. Poly(*N*-isopropylacrylamide): experiment, theory and application. *Prog. Polym. Sci.* 1992, 17, 163-249.
- [7] Castro Lopez, V.; Raghavan, S. L.; Snowden, M. J. Colloidal microgels as transdermal delivery systems. *React. Funct. Polym.* 2004, 58, 175-185.
- [8] Cornelius, V. J.; Snowden, M. J.; Silver, J.; Fern, G. R. A study of the binding of the biologically important hematin molecule to a novel imidazole containing poly(*N*-isopropylacrylamide) microgel. *React. Funct. Polym.* 2004, 58, 165-173.
- [9] Gerlach, G.; Guenther, M.; Suchanek, G.; Sorber, J.; Arndt, K.-F.; Richter, A. Application of sensitive hydrogels in chemical and pH sensors. *Macromol. Symp.* 2004, 210, 403-410.
- [10] Liu, H. Y.; Zhu, X. X. Lower critical solution temperatures of *N*-substituted acrylamide copolymers in aqueous solutions. *Polymer* 1999, 40, 6985-6990.
- [11] Hoare, T.; Pelton, R. Highly pH and Temperature Responsive Microgels Functionalized with Vinylacetic Acid. *Macromolecules (Washington, DC, U. S.)* 2004, 37, 2544-2550.
- [12] Schildknecht, C. E. *Allyl Compounds and Their Polymers*; Wiley-Interscience: New York, 1973.
- [13] Frisken, B.J. Revisiting the Method of Cumulants for the Analysis of Dynamic Light-Scattering Data. *Appl. Opt.* 2001, 40, 4087-4091.
- [14] Pusey, P. N.; Van Megen, W. Dynamic light scattering by non-ergodic media. *Phys. A (Amsterdam, Neth.)* 1989, 157, 705-741.
- [15] K. Schätzel Single-photon correlation techniques. In *Dynamic Light Scattering*, W. Brown, Eds.; Oxford University, Oxford, UK, 1993, pp 76-148.
- [16] Guillermo, A.; Cohen Addad, J. P.; Bazile, J. P.; Duracher, D.; Elaissari, A.; Pichot, C. NMR investigations into heterogeneous structures of thermosensitive microgel particles. *J. Polym. Sci., Part B: Polym. Phys.* 2000, 38, 889-898.

- [17] Stieger, M.; Richtering, W.; Pedersen, J. S.; Lindner, P. Small-angle neutron scattering study of structural changes in temperature sensitive microgel colloids. *J. Chem. Phys.* 2004, *120*, 6197-6206.
- [1] Meyer, S.; Richtering, W. Influence of Polymerization Conditions on the Structure of Temperature-Sensitive Poly(N-isopropylacrylamide) Microgels. *Macromolecules (Washington, DC, U. S.)* 2005, *38*, 1517-1519.
- [19] Shibayama, M.; Tanaka, T.; Han, C. C. Small angle neutron scattering study on poly(N-isopropyl acrylamide) gels near their volume-phase transition temperature. *J. Chem. Phys.* 1992, *97*, 6829-6841.
- [20] Shibayama, M.; Tanaka, T.; Han, C. C. Small-angle neutron scattering study on weakly charged temperature sensitive polymer gels. *J. Chem. Phys.* 1992, *97*, 6842-6845.
- [21] Shibayama, M. Spatial inhomogeneity and dynamic fluctuations of polymer gels. *Macromol. Chem. Phys.* 1998, *199*, 1-30.
- [22] Mears, S. J.; Deng, Y.; Cosgrove, T.; Pelton, R. Structure of Sodium Dodecyl Sulfate Bound to a Poly(NIPAM) Microgel Particle. *Langmuir* 1997, *13*, 1901-1906.
- [23] Crowther, H. M.; Saunders, B. R.; Mears, S. J.; Cosgrove, T.; Vincent, B.; King, M.; Yu, G. E. Poly(NIPAM) microgel particle de-swelling: a light scattering and small-angle neutron scattering study. *Colloids Surf., A* 1999, *152*, 327-333.
- [24] Saunders, B. R.; Crowther, H. M.; Morris, G. E.; Mears, S. J.; Cosgrove, T.; Vincent, B. Factors affecting the swelling of poly(N-isopropylacrylamide) microgel particles: fundamental and commercial implications. *Colloids Surf., A* 1999, *149*, 57-64.
- [25] Zubov, V. P.; Kumar, M. V.; Masterova, M. N.; Kabanov, V. A. Reactivity of Allyl Monomers in Radical Polymerization. *J. Macromol. Sci., Part A: Pure Appl. Chem.* 1979, *13*, 111-131.

Chapter III

DNA hybridization process on PNIPAM-VAA microgels particles

INTRODUCTION

DNA not only serves as a carrier of generic information in living organisms, but also finds important applications in many areas such as disease diagnosis [1, 2], gene therapy [3, 4, 5, 6, 7], biosensor [8, 9, 10, 11], and nanotechnology [12, 13, 14, 15, 16].

In many cases, DNA is combined with suitable polymers or solid supports to achieve its full potential. DNA microarrays have become useful tools in genomic studies and drug discovery [17, 18]. Unlike other hybridization formats, microarrays allow significant miniaturization, as thousands of different DNA fragments or oligonucleotide probes can be spotted onto a solid support. Therefore, this technology is ideal for extensive gene profiling studies and multiplexed detection of nucleic acids for diagnostic purpose. In fact, DNA microarray is one good example where DNA is immobilized onto a solid support to facilitate simultaneous analysis of all RNA transcripts in a given organism [19, 20]. Therefore, surface immobilization of nucleic acids

is one of the most important criteria to consider for developing DNA based bioassays or detection technology.

In recent years, latex colloidal particles with submicron size have been shown to be suitable materials for the surface immobilization of biomolecules such as proteins and DNA, through both physical adsorption and covalent coupling [21, 22]. The large area, low dispersity, and versatility of functional groups on the surface make colloidal particles particularly desirable for this purpose. It has been shown that cationic latex particles conjugated to DNA oligonucleotides can be used in the Enzyme Link Oligonucleotide Sorbent Assay (ELOSA) technique to detect nucleic acids with increased sensitivity [21, 22, 23]. Among the colloidal particles, PNIPAM microgels are a class of cross-linked colloidal particles possessing interesting physical properties of swelling and shrinking under external stimuli. Because of these attractive properties, PNIPAM microgels have been extensively investigated for use in many biomedical and industrial applications as already discussed in Chapter 1.

In this chapter we set out to investigate whether DNA conjugated microgels were compatible with hybridization process, that is commonly used for manipulations of DNA in the design of DNA bioassays or biosensors. First, we performed a Quenching experiment, in order to investigate the nature of the interaction of DNA fragments with microgel (physisorption *vs* hybridization) and thus, the specificity of hybridization on microgels.

Quenching of a fluorophore can occur as a result of the formation of a non-fluorescent complex between a fluorophore and another fluorophore or non-fluorescent molecule. This mechanism is known as “contact quenching” [24]. In contact quenching two molecules interact by proton-coupled electron transfer through the formation of hydrogen bonds. In aqueous solutions electrostatic, steric, and hydrophobic forces control the formation of hydrogen bonds. When this complex absorbs energy from light, the excited

state immediately returns to the ground state without emission of a photon and the molecules do not emit fluorescent light. Thanks to the nature of this phenomenon the fluorescence emission switch off can be the result of hybridization and does not occur in case of aspecific absorption on microgel surface.

Thus, Cy5-labeled DNA oligonucleotide was conjugated with PNIPAM-VAA particles and by using a full complementary DNA oligonucleotide, opportunely modified with Black Hole Quencher 2 (BHQ-2), we performed the quenching experiment. Once confirmed the capability of DNA conjugated microgels to catch and recognize specifically complementary DNA strands we analyzed the effect of temperature and pH on the hybridization event and its stability.

3.1 MATERIALS AND METHODS

3.1.1 Materials

1-Ethyl-3-(3-dimethylaminopropyl)carbodiimide (EDC) and 2-(*N*-morpholino)ethanesulfonic acid (MES) were provided by Aldrich. DNA oligonucleotides reported in Table 3.1 were purchased from Diatech-Eurogenetec. Tris(hydroxymethyl)aminomethane (TRIS) was provided by Applichem. Water used was from Millipore Milli-Q grade.

Table 3.1 List of oligonucleotide sequences used to test the hybridization process on PNIPMA-VAA microgel particles.

Name	Sequence 5'→3'	5' modification	3' modification	T _{melting} [°C]
Cy5-DNA	ACC-CGG-GTA- AGG-AAA-CAA- CTG-TAG-G	AMINE C6	Cy 5	54.2
BHQ-complementary	CCT-ACA-GTT- GTT-TCC-TTA- CCC-GGG-T	BHQ-2	-	54.2
BHQ-random	TCC-ATG-GTT- CAG-ACG-TTG- CAT-GCT-G	BHQ-2	-	54.2
FITC-complementary	CCT-ACA-GTT- GTT-TCC-TTA- CCC-GGG-T	6-FITC	-	54.2
FITC-random	TCC-ATG-GTT- CAG-ACG-TTG- CAT-GCT-G	6-FITC	-	54.2

3.1.2 DNA conjugation on PNIPAM-VAA microgel particles

1 mg of PNIPAM-VAA microgels were left overnight in 250 μ L of the buffer solution (MES, pH 4.8). The coupling reaction was carried out at 4 °C: EDC (0.05 M, final concentration, dissolved in the coupling buffer that was freshly prepared just before use) was added to the buffer solution, followed by the addition of 500 pmol Cy5-DNA oligonucleotide (see Table 3.1). The

total volume reaction was 0.5 mL. The reaction solution was covered with alumina and left overnight on a shaker at 4 °C. The reaction mixture of Cy5-DNA conjugated microgel was then precipitated down by ultra-centrifugation at 50000 rpm for 50 min. at room temperature. Precipitant was re-suspended in 1 mL of Milli-Q water. This washing step was repeated three more times. The microgels were resuspended at a final concentration of ~1 mg/mL. A control experiment was done using the same procedure but without EDC being added.

3.1.3 Spectrofluorimetry

For the design of fluorescent hybridization probes that utilize contact quenching, it is reported in literature that Cy5 is best quenched by the BHQ-2 (Figure 3.1) [25]. Thus, BHQ-2 quencher was set both on two different oligonucleotides: 1) BHQ-complementary, the complementary sequence to Cy5-DNA; 2) BHQ-random, for which the sequence is random and well chosen in order to avoid any type of interaction with Cy5-DNA (see Table 3.1).

The quenching experiment with BHQ-complementary/BHQ-random and Cy5 DNA strands was previously tested in solution in order to ascertain the electronic interaction of the two fluorescent probes. 20 pmol of Cy5-DNA were mixed to 20 pmol of BHQ-complementary in 0.1 M TRIS, pH 8 buffer in a final volume of 200 μ L and incubated at 25°C for 90 min. The specificity of the quenching event was evaluated by using BHQ-random oligonucleotide. Each sample was loaded onto a 96-well microplate and the fluorescence emission intensity was measured in 2300 EnSpire multilabel reader (Perkin-Elmer, Waltham, MA) by setting the $\lambda_{\text{ex(cyanine5)}}=633$ and $\lambda_{\text{em(cyanine5)}}=650$. The quenching efficiency was evaluated by comparing the fluorescence emission in presence of BHQ-complementary with the fluorescence of Cy5-

DNA oligonucleotide alone. The fluorescence emission measured in presence of BHQ-random oligonucleotide was used to evaluate the presence of aspecific interaction. The experimental uncertainties indicated represent the standard deviation of three replicates.

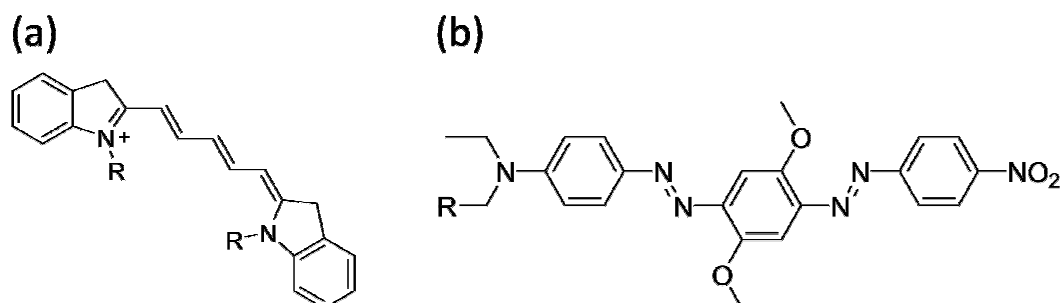


Figure 3.1: Molecular structure of Cy5 (a) and BHQ-2 (b).

3.1.4 Quenching experiments on Cy5-DNA coupled PNIPAM-VAA microgels particles.

Quenching solutions were prepared diluting 0.050 mL of Cy5-DNA conjugated microgels (1 mg/mL) in 0.450 mL of pH 8, 0.1 M TRIS buffer. Successively, 14 pmol of the BHQ-complementary/BHQ-random were added to the solution and incubated for 10 min at 25 °C. 200 μ L aliquots of quenched particles were analyzed by confocal microscopy ($\lambda_{\text{ex(cyanine5)}} = 633\text{nm}$; $\lambda_{\text{em(cyanine5)}} = 650\text{nm}$).

3.1.5 Hybridization on PNIPAM-VAA microgel coupled with Cy5-DNA

Hybridization solutions were prepared diluting 0.050 mL of Cy5-DNA conjugated microgels (1 mg/mL) in 0.450 mL of 0.1 M TRIS buffer. Then, 14 pmol of the DNA were added to the solution for 10 min. to allow the DNA hybridization. We tested the hybridization process with two fluoresceine labeled DNA sequences: the complementary sequence, named FITC-complementary, and the random one, FITC-random (see Table 3.1).

Hybridization process on PNIPAM-VAA microgels coupled with Cy5-DNA was analyzed as function of temperature in two sets of experiments: 1) the hybridization was carried out on Cy5-DNA conjugated PNIPAM-VAA microgels at 25 °C at two different pH values (pH 3 and pH8). Successively, the microgels were analyzed over an increasing temperature range (25, 30, 35, 40, and 45°C); 2) different aliquots of Cy5-DNA conjugated PNIPAM-VAA microgels were heated at different temperatures (25, 30, 35, 40 and 45 °C) at which the hybridization was carried out. In this case we analyzed microgels hybridization process only at pH 8. For each experiment 200 µL aliquots of hybridized particles were analyzed by confocal microscopy ($\lambda_{\text{ex(fluoresceine)}} = 488 \text{ nm}$; $\lambda_{\text{em(fluoresceine)}} = 530 \text{ nm}$).

3.1.6 CLSM imaging for fluorescence quantification

200 µl of microgels diluted solution (~0.1 mg/mL) from the quenching experiment and hybridization experiment (paragraphs 3.1.4 and 3.1.5) were loaded onto thermal chamber, illuminated at confocal laser scanning microscope Leica SP5 using Helium Neon laser 633 nm, Argon laser 488 nm and fluorescence images of microgel were collected. Objective: HCX PL APO CS 40.0x1.10 water, section thickness 1.2 µm, scan speed 700 Hz,

Excitation Laser Argon 488 nm, $\lambda_{\text{em(fluoresceine)}}$ range 500-530 nm, Excitation Laser Helium neon 633 nm, $\lambda_{\text{em(cyanine5)}}$ range 680-780 nm, image size 77.5x77.5 μm^2 .

For microgel experiments, 100 microparticles were selected for each sample to be analyzed and their fluorescence quantified. All captured images were analysed with a public domain image-processing Image J (version 1.43i, NIH, Bethesda, MD). Briefly the images were thresholded by Otsu algorithm and then processed with the Image J Analyze Particles function to computationally determine the number of single fluorescent particles sizing in the range of 1 μm . The fluorescence mean and standard deviation of each sample were calculated. The experimental uncertainty represents the standard error of the mean of three replicates measurements.

3.1.7 Dynamic Light Scattering Microgel Characterization

We determined the hydrodynamic radius of the particle using ALV – CGS-3 compact goniometer (ALV-Laser GmbH, Langen, Germany) operating at a wavelength of 633nm in vacuum and a time correlator ALV – LSE-5003 (ALV-Laser GmbH, Langen, Germany). From the measured time-average intensity correlation function, $g^{(2)}(q, \tau)$ the translational free diffusion is determined and the particle hydrodynamic radius extracted by common procedures [26]. We restricted the analysis to scattering angles $\theta = 40^\circ, 60^\circ, 80^\circ, 100^\circ, 120^\circ$.

3. 2 RESULTS AND DISCUSSION: STUDY OF THE HYBRIDIZATION PROCESS ON PNIPAM-VAA MICROGELS

Our investigative plan in this study is illustrated in Figure 3.3, which includes: 1) covalent coupling of 5'-amine modified Cy5-DNA oligonucleotide to carboxylic groups of PNIPAM-VAA microgels; 2) hybridization with a fluorescent probe (FITC-complementary/FITC-random). At the end of this process we analyzed the hybridization process as function of temperature by confocal microscopy imaging.

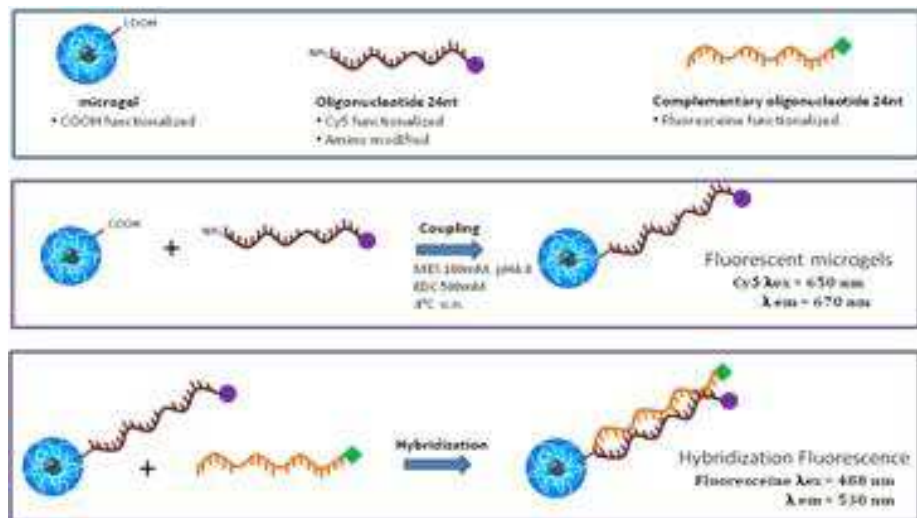


Figure 3.3: Schematic illustration of DNA coupling and hybridization on PNIPAM-VAA microgels.

We first synthesized the microgels as reported in Chapter 2. In order to confirm the covalent conjugation, the coupling reaction was conducted without EDC as control sample. After three washings of the particles, they were re-suspended in 1 mL of Milli-Q water and seen by confocal (Figure 3.4). The particle images show that the microgels control sample does not show any fluorescence emission (Figure 3.4a), ruling out any possible Cy5-DNA aspecific absorption on the particles.

We analyzed the effect of the hybridization on the PNIPAM-VAA hydrodynamic radius.

Two hybridization experiments were analyzed next by confocal microscopy: quenching experiment and the hybridization experiment are described below.

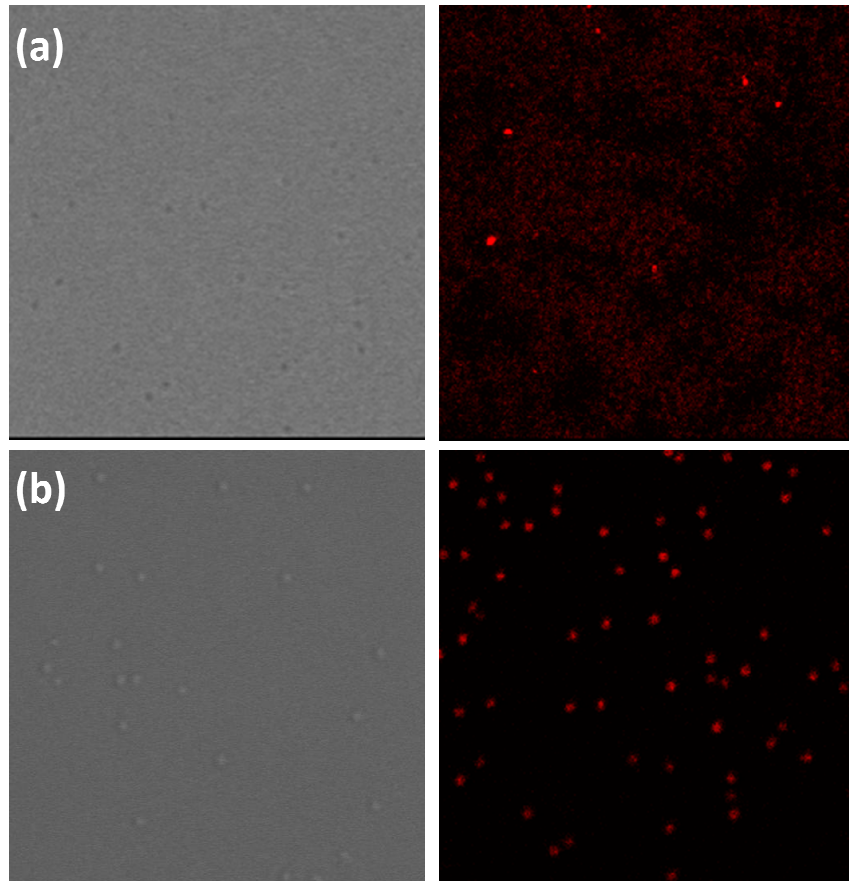


Figure 3.4: *Confocal images of PNIPAM-VAA particles after coupling reaction: (a) Cy5-DNA added in the coupling mixture without EDC; (b) Cy5-DNA coupled to PNIPAM-VAA particles via EDC reaction.*

3.2.1 Hydrodynamic Radii

The particle size and the shrinkage play an important role in the interaction of the microgel with oligonucleotide substrates, in terms of

surface extension and electronic interactions. As reported in Chapter 2, the effect of a polyelectrolyte conjugation, like in this case DNA or an oligonucleotide sequence, could suppress the microgels thermo-responsivity.

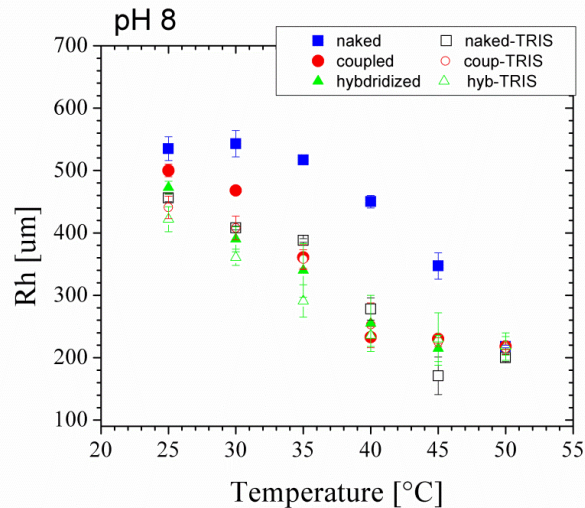


Figure 3.2: Size characterization by DLS of naked PNIPAM-VAA particles (blue squares); PNIPAM-VAA particles coupled with Cy5-DNA (red circles); and PNIPAM-VAA particles.

The experimental data (Figure 3.2) shows the swelling profile for i) naked-, ii) Cy5-DNA coupled- and iii) FITC-complementary hybridized-PNIPAM-VAA microgels at pH 8 in H₂O and in TRIS buffer. Naked particles size profile at pH 8 is rather broad. Both core and shell are swollen and the VPTT is shifted up 45 °C as described in Chapter 2. In proximity of the phase transition the total radius in water decreases as function of temperature from ~531 nm to ~216 nm. As already reported by several authors [27, 28], the hydrodynamic radius of PNIPAM microgels depends on the nature and the concentration of the electrolyte. The addition of TRIS buffer and the effect of DNA coupling and hybridization do not produce a completely shrinkage of the hydrodynamic radius and do not suppress the microgel thermo-responsivity.

3.2.2 Cy5-DNA conjugated PIPAM-VAA microgels capability in catching specific DNA oligonucleotides: hybridization or adsorption?

The use of fluorescent nucleic acid hybridization probes that generates a fluorescence signal only when they bind to their target enables real-time monitoring of nucleic acid detection assays. In the specific, the use of BHQ-2 quencher, attached both on the complementary oligonucleotide sequence to Cy5-DNA and on the random one, allowed us to investigate the specificity of hybridization process on Cy5-DNA PIPAM-VAA conjugated microgels.

We first validated the DNA probe design by evaluating the quenching efficiency of the Cy5-DNA oligonucleotide in solution in presence of the complementary and non complementary oligonucleotide. The Figure 3.5a reports the Cy5-DNA emission fluorescence in presence of the BHQ-complementary and BHQ-random oligonucleotide sequence. In presence of BHQ-random, Cy5-DNA maintains the same fluorescence emission value, which drops when in presence of the complementary sequence, BHQ-complementary.

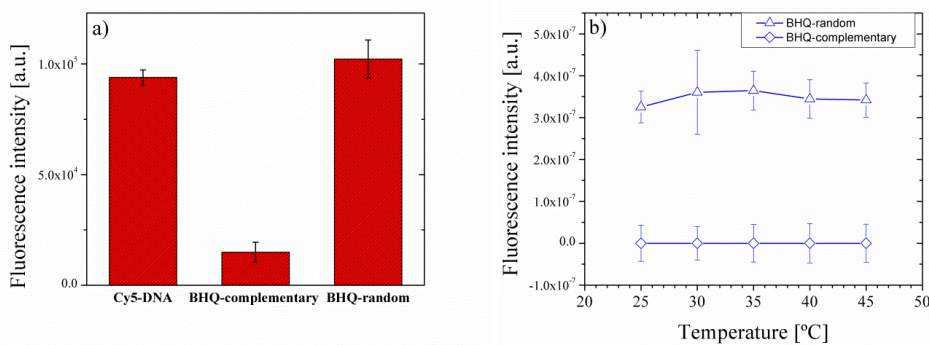


Figure 3.5: *Quenching experiment performance: (a) Fluorescence intensity at 25°C of Cy5-DNA free, in presence of BHQ-complementary and in presence of BHQ-random oligonucleotide in solution. (b) Fluorescence intensity of Cy5-DNA conjugated on the PNIPAM-VAA microgels as function of temperature in presence of BHQ-complementary or BHQ-random oligonucleotide sequence.*

Then the quenching experiment was performed on Cy5-DNA conjugated microgel in order to evaluate their ability to specifically hybridize the complementary DNA strand. The experiment was performed by incubating the Cy5-DNA conjugated microgels with BHQ-complementary, or the random oligonucleotide sequence, BHQ-random. As shown in Figure 3.5b when BHQ-random is dispersed in solution, microgel particles still emit fluorescence which does not change with temperature. Otherwise adding BHQ-complementary, Cy5 fluorescence emission on PNIPAM-VAA particles surface turns off. This demonstrates that there is a direct interaction between the complementary sequence and the Cy5-DNA attached on the microgel surface. The two strands form a double strand structure and the hybridization process occurs on the particles surface.

3.2.3 Effect of temperature on on Cy5-DNA conjugated PNIPAM-VAA microgels hybridization

Hybridization process on PNIPAM-VAA microgels coupled with Cy5-DNA was analyzed as function of temperature and microgel shrinking in two sets of experiments. In the first experiment the temperature effect on the de-hybridization process was evaluated at two different pH, pH 3 and pH 8. In fact, as we reported in the Chapter 2, these two pH values correspond to two microgel structures: at pH 3 value, the external shell is completely collapsed on the core of the particle; at pH 8, shell and core are swollen and microgel reaches the largest degree of swelling. Our experiment was set to evaluate whether the different degrees of swelling of the microgels (in terms of different temperatures) at two different architectures could drive the de-hybridization process on the surface of PNIPAM-VAA microgel particles. In Figure 3.6 we show the FITC-complementary/FITC-random emission fluorescence measured on the particles heated up 45 °C. This temperature value is far away from the temperature value of 54.2 °C, which corresponds

to the Melting Temperature (T_{melting} , see Table 3.1) of used DNA oligonucleotides sequences. Both sequences interact with the microgel particles, for which it is possible to detect a fluorescence value. The interaction between Cy5-coupled PNIPAM-VAA microgels and FITC-random is aspecific and the fluorescence value measured on the particles is 4 times lower than the one measured using the complementary sequence. The quenching experiments discussed above demonstrated that the interaction between Cy5-coupled PNIPAM-VAA microgels and FITC-complementary is specific and the hybridization process occurs on the Cy5-DNA conjugated particles. Increasing temperature, the FITC fluorescence value measured on particles remain constant both for pH 3 and pH 8 values. This means that the particle shrinkage and the degree of swelling have no effects on the hybridization process. The fluorescence intensity at pH 3 results lower than the one at pH 8. This is due to the fact that FITC fluorophore is pH-sensitive.

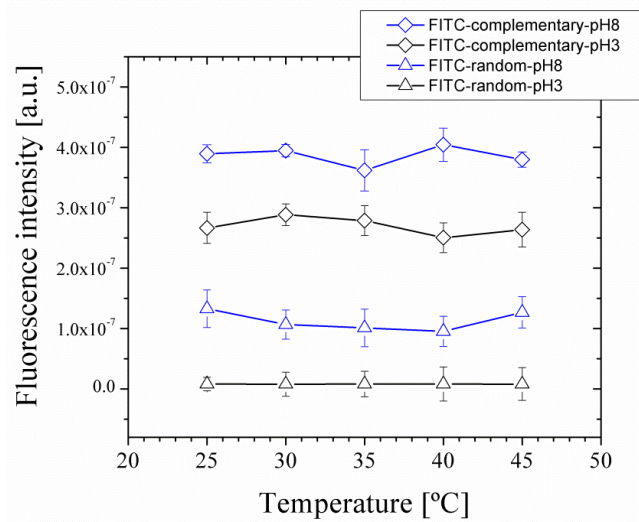


Figure 3.6: Fluorescence intensity measured on Cy5-DNA conjugated PNIPAM-VAA microgels incubated with FITC-complementary and FITC-random oligonucleotides as function of temperature and pH. FITC-complementary and FITC-random were added in the microgel solution before heating.

In the second experiment we analyzed the hybridization process as function of Cy5-DNA chains exposure on the microgel surface to the complementary and random oligonucleotide sequence. We performed hybridization process on Cy5-DNA coupled microgel, by adding FITC-complementary/FITC-random at different temperatures (25, 30, 35, 40 and 45 °C).

The analysis of the particles fluorescence emission is shown in Figure 3.7. Also in this case the emission fluorescence level measured on microgels is the same at each hybridization temperature tested. This result means that different exposure degree of Cy5-DNA does not have any effects on the hybridization in terms of process efficiency. The fluorescence emission f values measured in Figure 3.7 are comparable with the values shown in Figure 3.6.

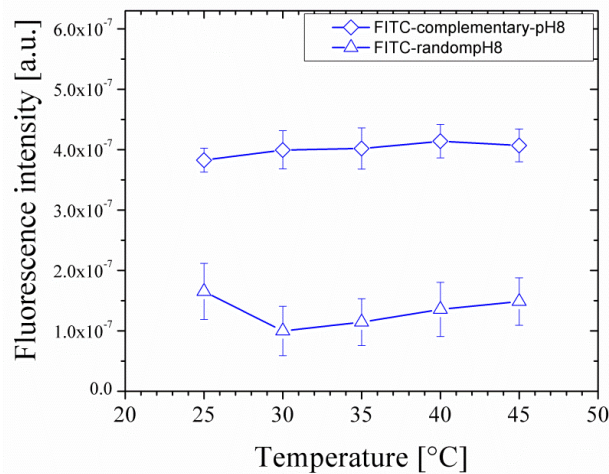


Figure 3.7: Fluorescence intensity measured on Cy5-DNA conjugated PNIPAM-VAA microgels incubated with FITC-complementary and FITC-random oligonucleotides at different temperatures. FITC-complementary and FITC-random were added in the microgel solution and the hybridization analyzed at each temperature tested (from 25 to 45 °C).

CONCLUSIONS

Thermo- and pH-responsive core-shell PNIPAM-VAA microgels were synthesized in order to perform the hybridization process on them. They were opportunely engineered with carboxylated functionalizations on the shell to conjugate amino modified DNA sequences. The hybridization process was performed and tested in terms of specific catching of a complementary oligonucleotide, ruling out any aspecific absorption on the microgel surface. Successively, the hybridization process was studied in details, looking at the effect of microgel structural changes.

The effect of the shrinkage controlled by temperature changes does not drive any de-hybridization process, whereas it affects the particle degree of swelling. No dependence of the hybridization process was highlighted during microgel conformation changing, neither when the shell has collapsed nor when it is fully extended outside the microgel. Eventually, even analyzing the process as function of the oligonucleotide exposure towards the complementary oligonucleotide sequence, there is no direct evidence of its effects on the interaction process between the two oligonucleotides.

REFERENCES

- [1] Jingming Bai, Kunihiro Yokoyama, Seigo Kinuya, Kazuhiro Shiba, Ryo Matsushita, Masaaki Nomura, Takatoshi Michigishi, and Norihisa Tonami. In vitro detection of *mdr1* mRNA in murine leukemia cells with ¹¹¹In-labeled oligonucleotide. *European Journal of Nuclear Medicine and Molecular Imaging*, 31(11):1523–1529, 2004.
- [2] B Tavitian. In vivo imaging with oligonucleotides for diagnosis and drug development. *Gut*, 52(suppl 4):40–47, 2003.
- [3] Yann Fichou and Claude Ferec. The potential of oligonucleotides for therapeutic applications. *Trends in Biotechnology*, 24(12):563 – 570, 2006.
- [4] Bruno Bordier, M Perala-Heape, Genevieve Degols, Bernard Lebleu, Simon Litvak, Leila Sarih-Cottin, and Claude Helene. Sequence-specific inhibition of human immunodeficiency virus (hiv) reverse transcription by antisense oligonucleotides: comparative study in cell-free assays and in hiv-infected cells. *Proceedings of the National Academy of Sciences*, 92(20):9383–9387, 1995.
- [5] L James Maher III, Peter B Dervan, Barbara Wold, and E Wickstrom. Inhibition of dna/protein interactions by oligonucleotide-directed dna triple helix formation: Progress and prospects. *Prospects for Antisense Nucleic Acid Therapy of Cancer and AIDS*, pages 227–242, 1991.
- [6] Jennifer F Lee, Gwendolyn M Stovall, and Andrew D Ellington. Aptamer therapeutics advance. *Current Opinion in Chemical Biology*, 10(3):282 – 289, 2006.
- [7] G. M. Emilsson and R. R. Breaker. Deoxyribozymes: new activities and new applications. *Cellular and Molecular Life Sciences CMLS*, 59(4):596–607, 2002.
- [8] Edward N. Brody and Larry Gold. Aptamers as therapeutic and diagnostic agents. *Reviews in Molecular Biotechnology*, 74(1):5 – 13, 2000.
- [9] Juewen Liu, Debapriya Mazumdar, and Yi Lu. A simple and sensitive dipstick test in serum based on lateral flow separation of aptamer-linked nanostructures. *Angewandte Chemie*, 118(47):8123–8127, 2006.
- [10] Rebecca Y. Lai, Kevin W. Plaxco, and Alan J. Heeger. Aptamer-based electrochemical detection of picomolar platelet-derived growth factor directly in blood serum. *Analytical Chemistry*, 79(1):229–233, 2007.
- [11] Naveen K Navani and Yingfu Li. Nucleic acid aptamers and enzymes as sensors. *Current Opinion in Chemical Biology*, 10(3):272 – 281, 2006.
- [12] Soong Ho Um, Jong Bum Lee, Nokyoung Park, Sang Yeon Kwon, Christopher C Umbach, and Dan Luo. Enzyme-catalysed assembly of dna hydrogel. *Nature materials*, 5(10):797–801, 2006.
- [13] Chenxiang Lin, Yan Liu, and Hao Yan. Self-assembled combinatorial encoding nanoarrays for multiplexed biosensing. *Nano Letters*, 7(2):507–512, 2007.

- [14] Yu He, Yi Chen, Haipeng Liu, Alexander E. Ribbe, and Chengde Mao. Self-assembly of hexagonal dna two-dimensional (2d) arrays. *Journal of the American Chemical Society*, 127(35):12202–12203, 2005.
- [15] Nadrian C Seeman. Dna nanotechnology: novel dna constructions. *Annual Review of Biophysics and Biomolecular Structure*, 27(1):225–248, 1998.
- [16] Yu He, Ye Tian, Alexander E. Ribbe, and Chengde Mao. Highly connected two-dimensional crystals of dna six-point-stars. *Journal of the American Chemical Society*, 128(50):15978–15979, 2006.
- [17] Christine Debouck and Peter N Goodfellow. Dna microarrays in drug discovery and development. *Nature genetics*, 21:48–50, 1999.
- [18] Matthew J Marton, Joseph L DeRisi, Holly A Bennett, Vishwanath R Iyer, Michael R Meyer, Christopher J Roberts, Roland Stoughton, Julja Burchard, David Slade, Hongyue Dai, et al. Drug target validation and identification of secondary drug target effects using dna microarrays. *Nature medicine*, 4(11):1293–1301, 1998.
- [19] Amit Dutt and Rameen Beroukhim. Single nucleotide polymorphism array analysis of cancer. *Current opinion in oncology*, 19(1):43–49, 2007.
- [20] Carolyn Miller Ling Wang Carl F. Edman Michael Nerenberg Westin, Xiao Xu. Anchored multiplex amplification on a microelectronic chip array. *Nature Biotechnology*, 18:199–204, Feb 1, 2000.
- [21] Teresa Basinska. Hydrophilic core-shell microspheres: A suitable support for controlled attachment of proteins and biomedical diagnostics. *Macromolecular Bioscience*, 5(12):1145–1168, 2005.
- [22] C. Pichot. Surface-functionalized latexes for biotechnological applications. *Current Opinion in Colloid & Interface Science*, 9(3):213 – 221, 2004.
- [23] Thierry Delair, Françoise Meunier, Abdelhamid Elaissari, Marie-Helene Charles, and Christian Pichot. Amino-containing cationic latex oligodeoxyribonucleotide conjugates: application to diagnostic test sensitivity enhancement. *Colloids and Surfaces A: Physicochemical and Engineering Aspects*, 153(13):341 – 353, 1999.
- [24] Salvatore AE Marras, Fred Russell Kramer, and Sanjay Tyagi. Efficiencies of fluorescence resonance energy transfer and contact-mediated quenching in oligonucleotide probes. *Nucleic acids research*, 30(21):e122–e122, 2002.
- [25] Salvatore A.E. Marras. Selection of fluorophore and quencher pairs for fluorescent nucleic acid hybridization probes. In Vladimir V. Didenko, editor, *Fluorescent Energy Transfer Nucleic Acid Probes*, volume 335 of *Methods in Molecular Biology*, pages 3–16. Humana Press, 2006.
- [26] Bruce J Berne and Robert Pecora. *Dynamic light scattering: with applications to chemistry, biology, and physics*. Courier Dover Publications, 2000.
- [27] Emma Daly and Brian R. Saunders. A study of the effect of electrolyte on the swelling and stability of poly(*n*-isopropylacrylamide) microgel dispersions. *Langmuir*, 16(13):5546–5552, 2000.

[28] Liusheng Zha, Jianhua Hu, Changchun Wang, Shoukuan Fu, and Meifang Luo. The effect of electrolyte on the colloidal properties of poly(*n*-isopropylacrylamide-co-dimethylaminoethylmethacrylate) microgel latexes. *Colloid and Polymer Science*, 280(12):1116–1121, 2002.

Chapter IV

High efficient SERS substrate formulation by self-assembled gold nanoparticles physisorbed on PNIPAM thermoresponsive hydrogels

INTRODUCTION

There is a big variety of analytical techniques that can be used for molecular detection of pollutants [1, 2] narcotics [3, 4] and bio-molecules for health and life science. Usually, the real samples are in complex media of compounds that need to be quantified. This problem is amplified when trace analyte detection is required, as signals from background molecules can overlap the signal of the analyte. One technique that holds great promise in this regard is Surface Enhanced Raman Spectroscopy (SERS). It is an extremely sensitive technique that can be tailored to provide the detection of specific analytes through their unique vibrational fingerprints [5]. The narrow line width of Raman spectra allows for multiple-analyte detection within complex mixtures, including detection down to the single molecule level [6, 7]. The enhancement of the Raman signal comes as a result of exciting localized surface plasmons within metallic nanostructures [8]. A further increase in the signal strength can be achieved by tailoring the metallic substrate, thereby lowering the limits of detection (LOD). This increment

comes mainly from the multiple hotspots that are being generated in a uniform fashion over a larger substrate producing high signal enhancement [9] across this area. There are various methods to fabricate such structures including lithographic [10, 11] and chemical approaches [12, 13]. However, minimizing the gap between particles or cavities and the complexity of substrate preparation -while maximizing uniformity- is crucial in optimizing the electromagnetic field enhancement [14]. Precise nanofabrication techniques capable of achieving these goals can be costly, time consuming and non-scalable.

In SERS, it is well known that the plasmonic coupling effect between nano-particles induces huge electromagnetic enhancement that allows SERS signals to be detected even with single-molecule sensitivity. Many studies have showed that small structures and gaps (around 10 nm) are required to generate the “hotspots” typically associated with high SERS activity [15, 16, 17]. Various approaches to prepare regular substrates with a plethora of hotspots for SERS detection have been demonstrated [18, 19, 20]. Actually, fabrication of uniform and efficient SERS substrates remains challenging due to the complex processes and high cost. So, it would be favorable to design and fabricate SERS substrates with a simple method that provides a much more uniform hotspot formation with high enhancement factors. The control of the inter-particle distance should be also desirable in order to optimize the Raman enhancement factor for each different experimental condition. In most cases, once Au nanoparticle assemblies are formed, the spatial distribution of Au nanoparticle building block is fixed. Thus, it is highly advantageous to fabricate responsive Au nanoparticle assemblies, in which the overall dimensions and inter particle spatial distances can respond to external stimuli.

During the past decade, intelligent hydrogels that can adjust their volume but also their properties in response to ambient stimuli have drawn enormous research interest in biomedical and pharmaceutical applications [21, 22].

Among them, PNIPAM has been detailed studied with regard to its well-known phase behavior in aqueous solutions, which has the sharpest transition in the class of thermo sensitive alkylacrylamide polymers [23, 24]. Indeed, it undergoes a reversible phase transition at about 32 °C in pure water from a swollen state to a shrunken state upon increasing temperature (see Chapter 1). These phase transitions in the PNIPAM hydrogel are expected to induce dramatic modifications in the optical properties of the substrate [25]. The seed growth of Ag and Au nanoparticles and nanorods in a PNIPAM hydrogel has been reported [26, 27, 28, 29] but sophisticated chemistry were required. PNIPAM were also used as a switch between the gold nanoparticles and the gold surface. However, most of the aforementioned approaches required complex and sophisticated chemistry for the conjugation of the gold nanoparticles on the surface of the hydrogels.

Herein, in this work we report on a robust, reproducible and easy to handle method for the engineering of PNIPAM-VAA thermo- and pH-responsive (see Chapter 2) hydrogel surfaces optimized for physisorption of gold nanoparticles and the fabrication of SERS active surfaces. These modes show the capability of tuning the interparticle distance and therefore control and modulate the SERS enhancement factor because hydrogels templates change their size upon temperature changing.

4.1 MATERIALS AND METHODS

4.1.1 Materials

1-Ethyl-3-(3-dimethylaminopropyl)carbodiimide (EDC) and 2-(*N*-morpholino)ethanesulfonic acid (MES) were purchased from by Sigma-

Aldrich and used as received. DNA oligonucleotide (5'-GCC-CAG-TAA-GGA-3') was 5'-amine modified and were purchased from Diatech-Eurogenetec. 40 nm gold nanoparticles was purchased from BBI. Water used in the synthesis and characterization was of Millipore Milli-Q grade.

4.1.2 DNA coupling reaction with PNIPAM-VAA microgels and absorption of gold nanoparticles

For the DNA coupling 1 mg of microgel particles were dissolved in MES buffer 0.1M at pH 4.5. Particles were left overnight in the buffer solution. The coupling reaction was carried out at 4 °C. EDC was added before the addition of 500 pmol DNA. Total volume reaction was 0.5 mL and EDC concentration was 0.5M. The reaction solution was covered with alumina and left overnight on a shaker at 4 °C. The reaction mixture of microgel-DNA conjugated was then precipitated down by ultra-centrifugation at 50000 rpm for 50 min at room temperature. Precipitant was re-suspended in 1 mL of Milli-Q water. After the coupling of PNIPAM-VAA microgels, gold nanoparticles were added to the solution and after 15 min of incubation were adsorbed on hydrogel.

4.1.3 UV-Vis absorption spectroscopic measurements

UV-Vis absorption spectroscopic measurements were performed on peptide-gold nanoparticles conjugates solutions placed in 1 cm path-length quartz optical cuvettes. Spectra were recorded with a Cary 100 UV-Vis spectrometer from 200 to 800. The estimated resolution was 1nm and background was corrected with Milli Q water.

4.1.4 Dynamic Light Scattering measurements

The Dynamic light scattering measurements were performed with an ALV – CGS-3 compact goniometer (ALV-Laser GmbH, Langen, Germany) operating at a wavelength of 633nm in vacuum and a time correlator ALV – LSE-5003 (ALV-Laser GmbH, Langen, Germany).

4.1.5 TEM micrographs

Electron microscopy samples were prepared on a 200 mesh fromvar copper TEM grids from Agar scientific. One drop of solution was applied to the grid from a pipette. After solution evaporation the grid was washed with deionized water in order to remove salt excess from grid surface. Scanning transmission electron microscopy was performed with a Cryo-TEM tomography TECHNAI 20 FEI COMPANY. The images were acquired on a Vacuum generator operated at 250KV with camera (FEI-EAGLE) exposure time of 1 second. The estimated point to point resolution was 2 Å.

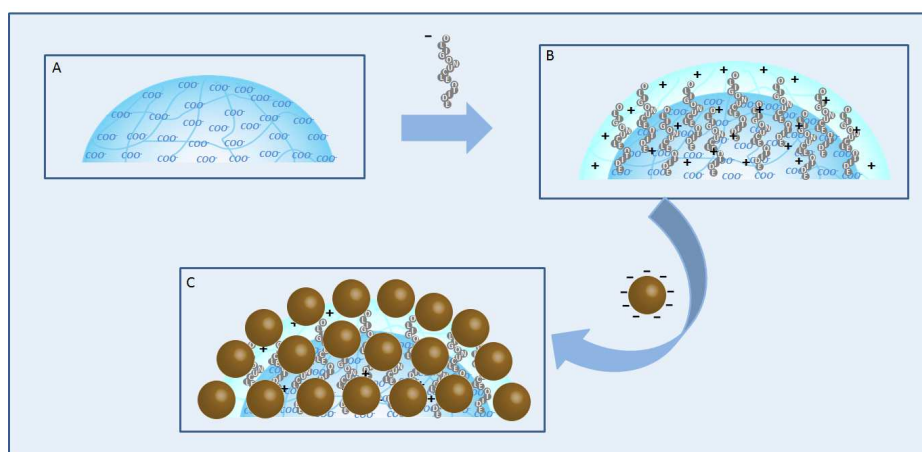
4.1.6 Raman spectroscopy

The Raman spectra were excited with a diode laser 780 nm. An 10x/x0,25 objective was utilized to focus the laser beam into the well plate which were filled with gold nano-colloidal suspensions. The Raman spectra were acquired with a DXR Raman spectrometer from Thermofischer Scientific with 20 mW laser power.

4.2 RESULTS AND DISCUSSION

As mentioned above, the advance of this approach consists in the simple mechanism by which the gold nanoparticles are adsorbed on a hydrogel template. More detailed, the PNIPAM-VAA microgel surface is engineered and optimized for the physisorption of gold nanoparticles. This physical adsorption is based on electrostatic interactions between the positive charge of engineered PNIPAM-VAA microgels and the negative charge of Au nanoparticles. The most important part of the study is that surface charge inversions have been taking place after the DNA coupling giving us the possibility for electrostatic based interactions between the hydrogels and the gold AuNPs. This charge inversion, which sounds very strange as far as on negative surface charged PNIPAM-VAA microgel attached also negative charged DNA strands, is based on the universal theory of charge inversion and the idea of a strongly correlated liquid of adsorbed counter-ions [30]. The absolute values of the ζ -potential measured before and after the DNA coupling was -25 and +20 respectively. The overall process is presented schematically in details in scheme 4.1 on which it is demonstrated the experimental procedure step by step. The great advantage of using DNA in order to inverse the surface charge of PNIPAM microgels is that DNA does not generate important SERS spectra. It is extremely important that the engineered and fabricated SERS surfaces possess the advantage for as much lower spectral background as possible; in our case the oligonucleotide plays this role successfully.

Scheme 4.1: *The experimental process for the engineering of PNIPAM-VAA thermo-responsive microgel surfaces optimized for physisorption of gold nanoparticles. A) as prepared PNIPAM-VAA microgels with negative surface charge because of the presence of the COO⁻, B) charge inversion after the coupling of the DNA and final on C) the surface loaded PNIPAM-VAA microgels with AuNPs.*



For the characterization of the PNIPAM-VAA-AuNPs composites, we started with the kinetics studies of this adsorption procedure. This study was of paramount interest because it will help to better understand the system, but also to decide for the appropriate experimental parameters. Therefore, 40 nm gold nanoparticles were added continuously in a PNIPAM-VAA microgel solution. UV-vis absorption spectra were acquired at each sample with the time and presented in Figure 4.1. We can see from both experimental procedures that the adsorption of AuNPs is fast and seems to stop for a ratio around 300 AuNPs per microgel. More specifically, we can see that there is a continuous shifting of the absorption band for the AuNPs ratio's 50, 100 and 150. At higher AuNPs concentrations (200 and 250) almost no changes were observed with time. Another important outcome of this experiment is that the adsorption at each one of the different AuNPs concentrations was fast as far as no more spectroscopic changes were observed after 15 min as clearly shown in the Figure 4.1. Finally, it was found that for even higher loading no

spectroscopic changes were appeared that means that no more AuNPs adsorbed on the hydrogel template. After this kinetic study, the conclusion was that the adsorption of AuNPs on PNIPAM-VAA microgels are a fast procedure and the maximum loading is found to be around 250.

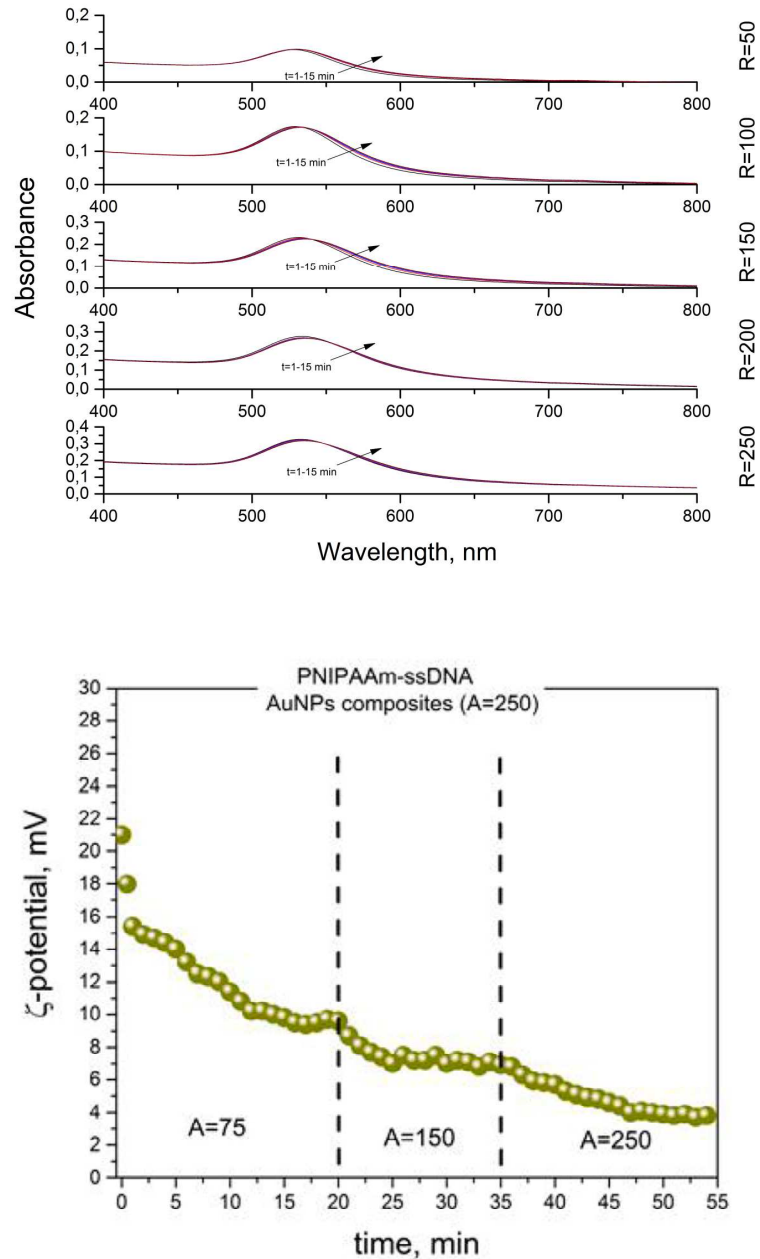


Figure 4.1: (Top) UV-vis absorption and (bottom) ζ -potential measurements at PNIPAM-VAA-Au composites at different 40 nm AuNPs loading with the time.

Similar results were found after ζ -potential measurements. Specifically, on PNIPAM–VAA–ssDNA with ζ -potential around 20 mV, AuNPs were added continuously and the ζ -potential was measured as a function of time. As seen in Figure 4.1, the ζ -potential drops with the time as long as the adsorption procedure continues. The biggest differences appeared at the first moments of the AuNP addition, and after 15 min, the changes were insignificant. We have also verified in this way that the maximum adsorption was around 250 AuNPs per microgel because the changes in ζ -potential were eliminated.

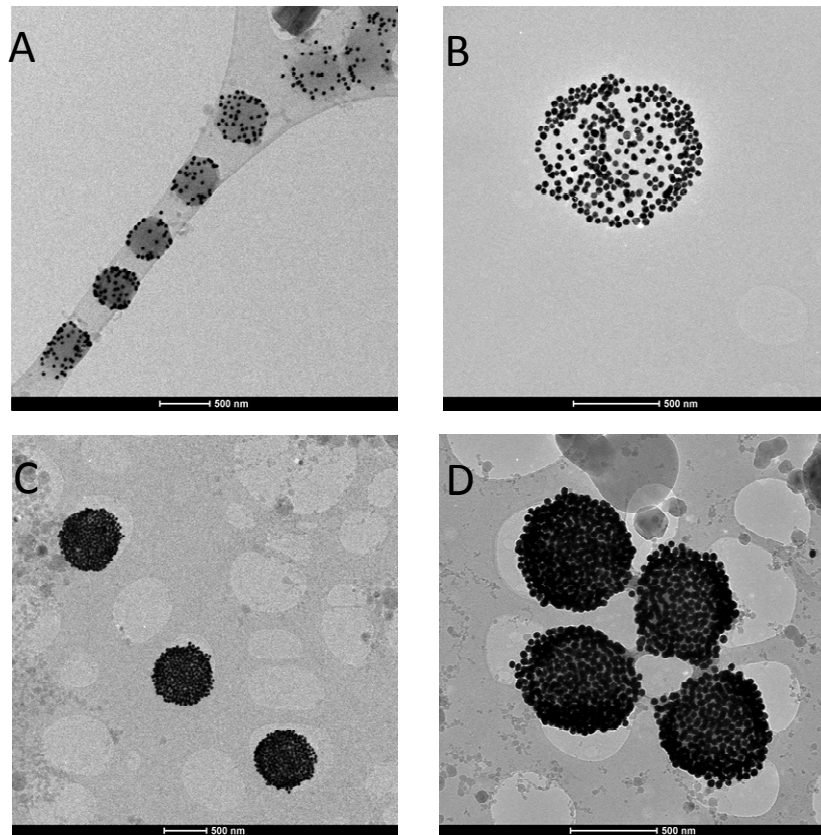


Figure 4.2: TEM images of PNIPAM-VAA-Au composites for different Au loading (A=50, B=150, C&D=250.)

Continuing, in Figure 4.2 we present the Transmission electron microscopy (TEM) images of PNIPAM-VAA microgels after the gold nanoparticle adsorption at different gold nanoparticle concentrations. Specifically, 50,150 and 250 AuNPs per PNIPAM-VAA microgels were added and the difference can be easily visualized by the TEM images. As it is

clearly demonstrated from Figure 4.2, the adsorption of AuNPs was successful at all of the different AuNPs loading. Furthermore, higher quantity of AuNPs added on the starting hydrogel solution means bigger amount of physisorbed AuNPs on the hydrogel template.

Thermoresponsive PNIPAM-VAA-Au composites were characterized by DLS. Figure 4.3 exhibits the variation of the hydrodynamic radius as the temperature changes from 15 to 40 °C for PNIPAM-VAA-Au templates with 250 AuNPs per hydrogel. The reversibility of this phase transition was also clearly demonstrated in this figure as far as the radius on 15 °C after the first heating cycle is almost the same as in the beginning. The critical temperature, where the radius changed rapidly, was at around 32 °C for our system. Since the measured LCST is similar to that of the pure PNIPAM-VAA microgel, the presence of vast Au nanoparticles does not significantly affect the swelling behavior of the PNIPAM-VAA template. Specifically, the radius on 15 °C for the totally swelled hydrogels measured 670 nm and for collapsed ones on 40 °C was around 390 nm, as demonstrated clearly in Figure 4.3.

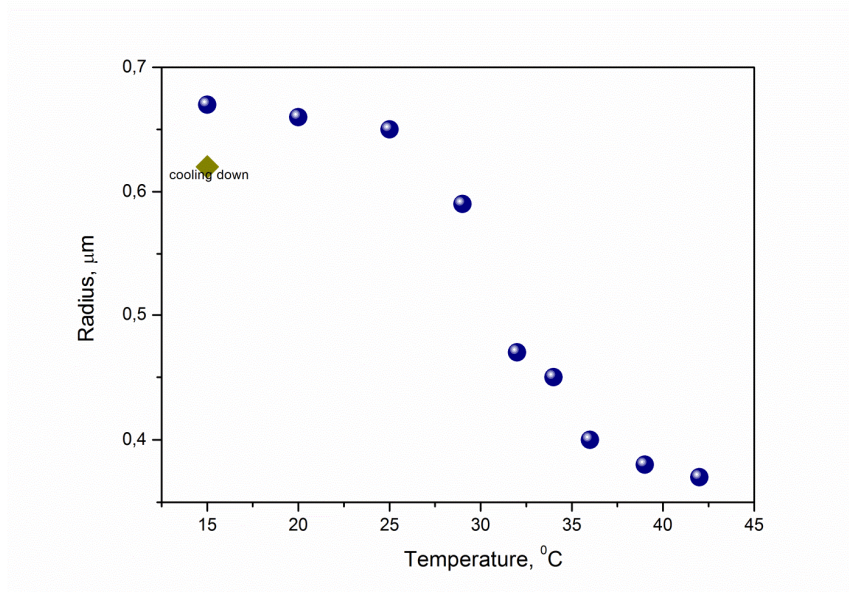


Figure 4.3: *Temperature dependence of the Radius of PNIPAM-VAA-Au composites for high AuNPS loading (250).*

In Figure 4.4 UV-vis absorption spectra were recorded on the aforementioned system at different temperatures (250 AuNPs per PNIPAM-VAA microogel). The difference on plasmon resonance of AuNPs on the PNIPAM-VAA microogel surface was crucial for the fabrication of SERS active substrates. In Figure 4.4 we present also the UV-vis absorption spectra at different temperatures. It is clearly demonstrated that, as temperature increases, the absorption band of AuNPs at 525 nm changes. In detail, a continuous broadening of the band is shown until the LCST; above this temperature changes were intense and a second band at a higher wavelength around 700 nm appeared. This band results from the coupling of surface plasmons between closely spaced particles. In aggregated colloids, the particles are physically connected, but it is essential to note that direct contact is not always needed to observe collective plasmon modes. In fact, even if the spacing between particles is narrowing compared to the wavelength of light, these collective plasmon modes can be observed. In this case, the interparticle spacing became narrow because of the decrease in the AuNPs-PNIPAM-VAA radius resulting in this new red shifted absorption band at ~ 700 nm.

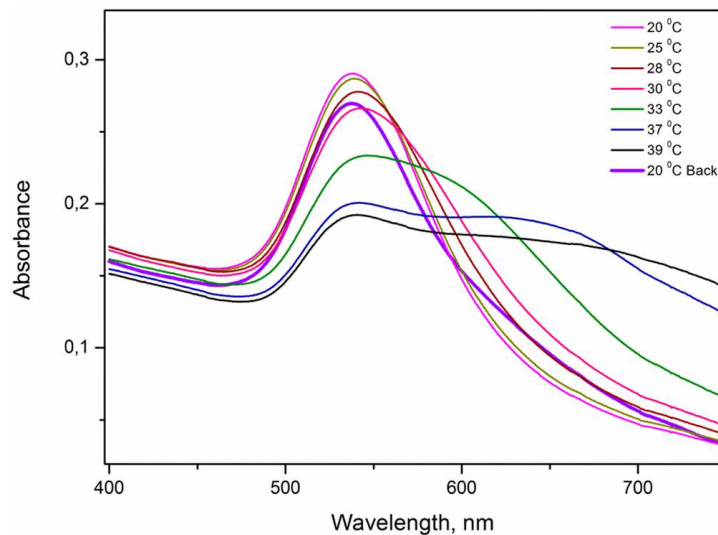


Figure 4.4: *UV-vis absorption spectra of PNIPAM-VAA-Au composites upon temperature changes.*

In order to better understand the dynamic changes that were taking place because of the hydrogel template shrinkage, the calculation of the interparticle distance between the adsorbed AuNPs was critical. Assuming uniform dispersed AuNPs on the hydrogel and having the scheme in the inset of Figure 4 in our mind, we calculated the interparticle distance between the gold nanoparticles at different temperatures. In detail, assuming cubes with dimension $80 + 2\delta$ as it is clearly shown from the scheme and calculating the area of these cubes knowing the total surface of the hydrogel, we can determine the δ , which gives the distance between two gold nanoparticles. For example, for 264 gold nanoparticles, there are 66 cubes in which these particles are placed (4 AuNPs per Cube). The area of each cube can be easily calculated and, as far as the area of the hydrogel at each temperature is already known from the DLS measurements, the interparticle distance was calculated for the high AuNPs loading (256 Au particles per hydrogel) - as demonstrated in Figure 4.5.

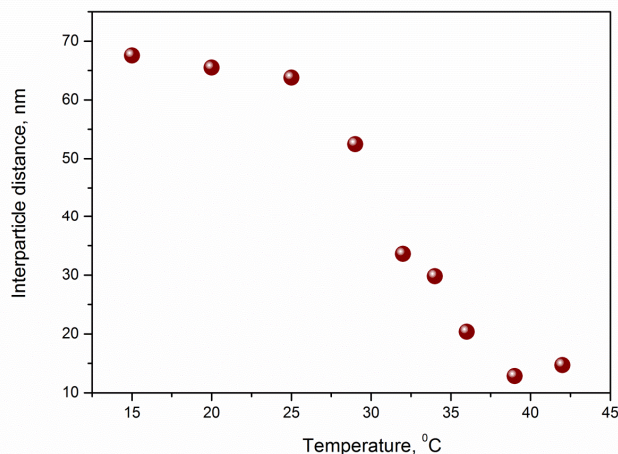


Figure 4.5: *The interparticle distance at different temperatures calculated assuming uniform dispersed gold nanoparticles on the PNIPAAm hydrogels surface.*

The SERS enhancement of the aforementioned PNIPAM-VAA-Au modes was tested using adenine as an analyte. 500 ng/mL of adenine solution were added in PNIPAM-VAA-Au composites and left some time in order to let the adenine molecules to adsorb on Au nanoparticles. Then 100 μ L of the aforementioned solution were added in a well plate and placed under the microscope. The spectra were collected using a 10X/xO,25 objective at different temperatures. The recorded spectra were presented in Figure 4.6 demonstrating the intensity dependence on the temperature. As it is clearly shown in the figure, the intensity of the adenines band at 735 wavenumbers at 20 $^{\circ}$ C is very low, but -as the temperature increased- the intensity also increased dramatically. Such a result was expected; when the radius of the composite decreases, the AuNPs comes closer, the hotspots are created, resulting in high enhancement on Raman spectra. In our case the enhancement factor changed from 104 to 106 upon temperature increase. It is also important to report the dependence of the intensity on the interparticle distance. It would be interesting to observe the appropriate interparticle distance for the higher enhancement on the Raman spectra. These results are presented in Figure 4.6, which demonstrate the intensity versus the inverse of the interparticle distance (for better observation). The interparticle distance with the higher enhancement was at around 15 nm, close to the theoretical studies that predict a hotspot generation at interparticle distances of around 10 nm [15, 16, 17].

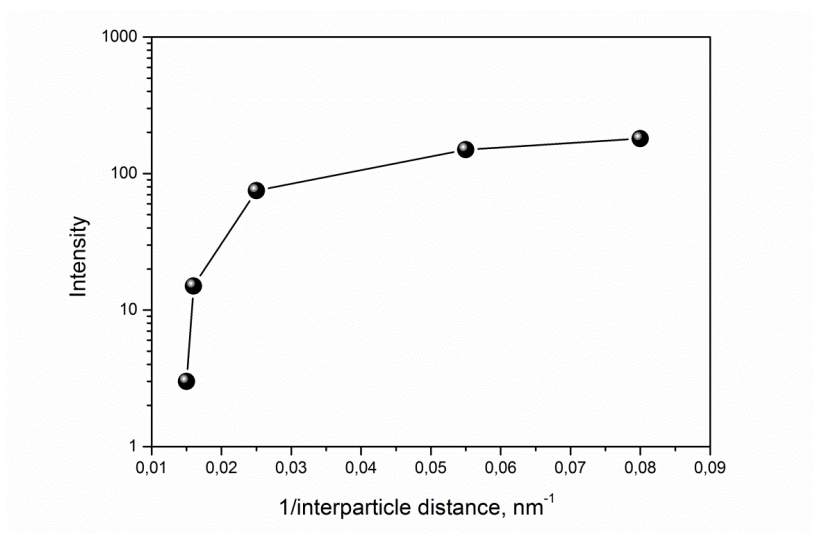
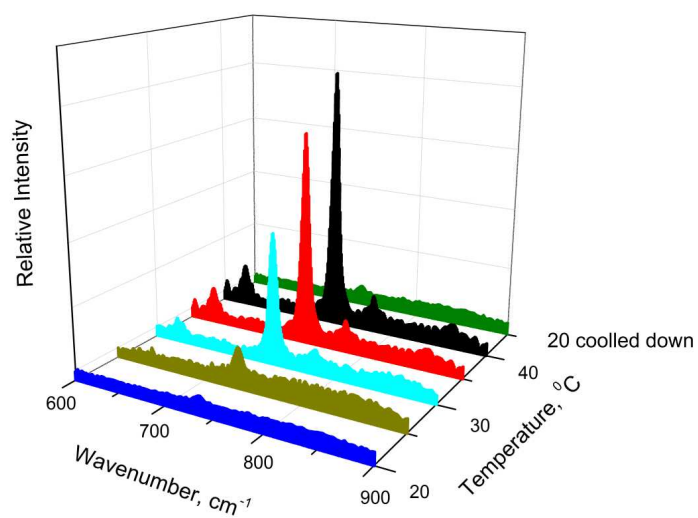


Figure 4.6: (Top) SERS spectra of 500ng/mL adenine solution at different temperatures and (bottom) the corresponding relationship between the logarithmic plot of SERS intensity at 735 cm⁻¹.

CONCLUSIONS

In conclusion, in this work we have presented a new, simple and reproducible method of physisorption of 40 nm gold nanoparticles on PNIPAM-VAA thermo- and pH-responsive microgels for the fabrication of highly efficient SERS substrates. We tuned the interparticle distance of the adsorbed gold nanoparticles because hydrogels matrixes changed their size upon temperature variations. We also studied the kinetics of this absorption and found that at around 15 min the process was rather finished. We performed a deep characterization with dynamic light scattering and UV-vis absorption spectroscopy for either the size or interparticle AuNPs observation upon temperature variation, or the optical characterization of the system. Finally, we collected SERS spectra and were able to verify the strong dependence of the intensity on the interparticle distance of the adsorbed AuNPs. These results stress the capability and the potentiality of the usage of smart polymer or even bio-polymer templates for SERS, but also for other plasmonic applications. The big advantage of these templates is that -beside the well-known role of concentrators- a second and much more crucial parameter that can enhance the information can be acquired from this concentrated analyte, the Raman spectra in our case; it offers the possibility for extreme low LOD.

REFERENCES

- [1] Lafevre, F.; Chalifour, A.; Yu, L.; Chodavarapu, V.; Juneau, P.; Izquierdo, R. Algal fluorescence sensor integrated into a microfluidic chip for water pollutant detection. *Lab on a Chip*, 2012, 12, 787-793.
- [2] Byer, R. L.; Garbuny, M. Pollutant Detection by Absorption Using Mie Scattering and Topographic Targets as Retroreflectors. *Appl. Opt.*, 1973, 12, 1496-1505.
- [3] Kawano, R.; Osaki, T.; Sasaki, H.; Takinoue, M.; Yoshizawa, S.; Takeuchi, S. Rapid Detection of a Cocaine-Binding Aptamer Using Biological Nanopores on a Chip. *J. Am. Chem. Soc.*, 2011, 133, 8474-8477.
- [4] Zhang, J.; Wang, L. H.; Pan, D.; Song, S. P.; Boey, F. Y. C.; Zhang, H.; Fan, C. H. Visual Cocaine Detection with Gold Nanoparticles and Rationally Engineered Aptamer Structures. *Small*, 2008, 4, 1196-1200
- [5] Manikas, A.C.; Soto Beobide, A.; Voyiatzis, G. A. Quantitative analysis via Surface Enhanced Raman Scattering from Ag nano-colloids utilizing an oscillating cell and right-angle collection geometry. *Analyst*, 2009, 134, 587-592.
- [6] Nie, S. M.; Emery, S. R. Probing single molecules and single nanoparticles by surface-enhanced Raman scattering. *Science*, 1997, 275, 1102-1106
- [7] Kneipp, K.; Wang, Y.; Kneipp, H.; Perelman, L. T.; Itzkan, I.; Dasari, R.; Feld, M. S. Single Molecule Detection Using Surface-Enhanced Raman Scattering (SERS). *Phys. Rev. Lett.*, 1997, 78, 1667-1670.
- [8] Kelly, K. L.; Coronado, E.; Zhao, L. L.; Schatz, G. C. The optical properties of metal nanoparticles: The influence of size, shape, and dielectric environment. *J. Phys. Chem. B*, 2002, 3, 668-677.
- [9] Dadosh, T.; Sperling, J.; Bryant, G. W.; Breslow, R.; Shegai, T.; Dyshel, M.; Haran, G.; Bar-Joseph, I. Plasmonic Control of the Shape of the Raman Spectrum of a Single Molecule in a Silver Nanoparticle Dimer. *ACS Nano*, 2009, 3, 1988-1994.
- [10] Yan, B.; Thubagere, A.; Premasiri, W. R.; Ziegler, L. D.; Dal Negro, L.; Renhard, B. M. Engineered SERS Substrates With Multiscale Signal Enhancement: Nanoparticle Cluster Arrays *ACS Nano*, 2009, 3, 1190-1202.
- [11] Kahl, M.; Voges, E.; Kostrewa, S.; Viets, C.; Hill, W. Periodically structured metallic substrates for SERS. *Sens. Actuat. B*, 1998, 51, 285-291.
- [12] Chen, A. Q.; DePrince, A. E.; Demortiere, A.; Joshi-Imre, A.; Shevchenko, E. V.; Gray, S. K.; Welp, U.; Vlasko-Vlasov, V. K. Self-Assembled Large Au Nanoparticle Arrays with Regular Hot Spots for SERS. *Small*, 2011, 7, 2365-2371.
- [13] Manikas, A. C.; Causa, F.; Della Moglie, R.; Netti, P.A. Tuning Gold Nanoparticles Interface by Specific Peptide Interaction for Surface Enhanced Raman Spectroscopy (SERS) and Separation Applications. *ACS Applied Materials & Interfaces*, 2013, 5, 7915-7922.

- [14] Yang, Z-L.; Li, V.; Ren, B.; Tian, Z-Q. Tunable SERS from aluminium nanohole arrays in the ultraviolet region. *Chem. Commun.*, 2011, 47, 3909-3911.
- [15] Lim, D. K.; Jeon, K. S.; Kim, H. M.; Nam J. M.; Suh, Y. D. Nanogap-engineerable Raman-active nanodumbbells for single-molecule detection. *Nat. Mater.*, 2010, 9, 60-67.
- [16] Lee, A.; Andrade, G. F. S.; Ahmed, A.; Souza, M. L.; Coombs, N.; Tumarkin, E.; Liu, K.; Gordon, R.; Brolo, A. G.; Kumacheva, E. Probing Dynamic Generation of Hot-Spots in Self-Assembled Chains of Gold Nanorods by Surface-Enhanced Raman Scattering. *J. Am. Chem. Soc.*, 2011, 133, 7563-7570.
- [17] Moskovits, M. SPECTROSCOPY Expanding versatility. *Nature*, 2010, 464, 357-357.
- [18] Tang, H. B.; Meng, G. W.; Huang, Q.; Zhang, Z.; Huang Z. L.; Zhu, C. H. Arrays of Cone-Shaped ZnO Nanorods Decorated with Ag Nanoparticles as 3D Surface-Enhanced Raman Scattering Substrates for Rapid Detection of Trace Polychlorinated Biphenyls. *Adv. Funct. Mater.*, 2012, 22, 218-224.
- [19] Lim, D. K.; Jeon, K. S.; Hwang, J. H.; Kim, H.; Kwon, S.; Suh Y. D.; Nam, J. M. highly uniform and reproducible surface-enhanced Raman scattering from DNA-tailorable nanoparticles with 1-nm interior gap. *Nat. Nanotechnol.*, 2011, 6, 452-460.
- [20] Cecchini, M.P.; Turek, V.A.; Paget, J.; Kornyshev, A. A.; Edel, J. B. Self-assembled nanoparticle arrays for multiphase trace analyte detection. *Nature materials*, 2013, 12, 165-172.
- [21] Wu, D. Q.; Sun, Y. X.; Xu, X. D.; Cheng, S. X.; Zhang X. Z.; Zhuo, R. X. Biodegradable and pH-sensitive hydrogels for cell encapsulation and controlled drug release. *Biomacromolecules*, 2008, 9, 1155-1162.
- [22] Zhang, J.; Peppas, N. A. Synthesis and characterization of pH- and temperature-sensitive poly(methacrylic acid)/poly(N-isopropylacrylamide) interpenetrating polymeric networks. *Macromolecules*, 2000, 33, 102-107.
- [23] Wu, T.; Zhang, Q. Q.; Hu, J. M.; Zhang G. Y.; Liu, S. Y. Composite silica nanospheres covalently anchored with gold nanoparticles at the outer periphery of thermoresponsive polymer brushes. *J. Mater. Chem.*, 2012, 22, 5155-5163.
- [24] Kim J. H.; Lee, T. R. Hydrogel-templated growth of large gold nanoparticles: Synthesis of thermally responsive hydrogel-nanoparticle composites. *Langmuir*, 2007, 23, 6504-6509.
- [25] Alvarez-Puebla, R. A.; Contreras-Caceres, R.; Pastoriza-Santos, I.; Perez-Juste, J.; Liz-Marzan, L. M. Au@pNIPAM Colloids as Molecular Traps for Surface-Enhanced, Spectroscopic, Ultra-Sensitive Analysis. *Angew. Chem., Int. Ed.*, 2009, 48, 138-143.
- [26] Lu, Y.; Liu G. L.; Lee, L. P. High-density silver nanoparticle film with temperature-controllable interparticle spacing for a tunable surface enhanced Raman scattering substrate. *Nano Lett.*, 2005, 5, 5-9.

- [27] Wu, Y.; Zhou, F.; Yang, L.; Liu, J. A shrinking strategy for creating dynamic SERS hot spots on the surface of thermosensitive polymer nanospheres. *ChemComm*, 2013, *49*, 5025-5027.
- [28] Lee, J. H.; Mahmoud, M.A.; Sitterle, V. B.; Sitterle, J.J.; Meredith, C. Highly scattering, Surface –Enhanced Raman Scattering-active, metal nanoparticle-coated polymers prepared via combined swelling-heteroaggregation. *Chem Mater.*, 2009, *21*, 5654-5663.
- [29] Khan, A.; Alhoshan, M. Preparation and characterization of pH-responsive and thermoresponsive hybrid microgel particles with gold nanorods. *Polymer chemistry*, 2013, *51*, 39-46.
- [30] Yu Grosberg, A.; Nguyen, T. T.; Shklovskii, B. I. Colloquium: The physics of charge inversion in chemical and biological systems. *Reviews in Modern Physics*, 2002, *74*, 329-345.